Mechanization of scalar field theory in 1+1 dimensions

Filip Blaschke[1,*] and Ondřej Nicolas Karpíšek[2]

[1]*Research Centre for Theoretical Physics and Astrophysics, Institute of Physics, Silesian University in Opava, Bezručovo nám. 1150/13, 746 01 Opava, Czech Republic*
[2]*Institute of Physics, Silesian University in Opava, Bezručovo nám. 1150/13, 746 01 Opava, Czech Republic*
*E-mail: fblasch@post.cz

....
"Mechanization" is a procedure of replacing a scalar field in 1+1 dimensions with a piece-wise linear function, i.e. a finite graph consisting of N joints (vertices) and straight segments (edges). As a result, the field theory is approximated by a sequence of algebraically tractable, general-purpose collective coordinate mechanical models. We observe the step-by-step emergence of dynamical objects and associated phenomena as N increases. "Mech-kinks" and "mech-oscillons"—mechanical analogs of kinks and oscillons (bions)—appear in the simplest models, while more intricate dynamical patterns, such as the bouncing phenomenon and bion pair-production, emerge gradually as decay states of high-N mech-oscillons.
....
Subject Index   A11

1. Introduction

The scattering of solitons provides a unique window on the inner workings of non-linear field theories. Even in the case of the simplest solitons, kinks, the rich phenomenology that we see is not yet completely understood despite four decades of theoretical research [1–14].

The prototypical non-linear field theory is the ϕ^4 model with a single scalar field and double-well potential $V(\phi) = \frac{1}{2}\left(1 - \phi^2\right)^2$, where the kink solution has an especially simple form: $\phi_K(x) = \tanh(x)$. Numerical investigations of kink (K) anti-kink ($\bar{K}$) collisions reveal an intricate pattern of possible outcomes [1–4,11,13]: (i) Above the critical velocity $v_{\text{crit}} \approx 0.26$, the colliding pair is immediately reflected and escapes to infinity. (ii) Below this threshold, the solitons sometimes form a "bound state" (bion) that slowly decays to the vacuum via the emission of radiation. (iii) Before final reflection and escape to infinity, the kink and anti-kink bounce off each other several times. These bounces occur in narrow windows of initial velocities that are nested and fractal-like, punctuated by "bion chimneys," and are observed only for initial velocities larger than $v_{\text{min}} \approx 0.18$.

Understanding these phenomena is, at its core, a problem of complexity. During $K\bar{K}$ collisions, the field enters a deeply non-linear regime, where our analytic and "weak-field"

perturbative tools fail. It could be the case that a very large number of degrees of freedom participate with equal importance, and we may never untangle the web of inner dependencies. That would be a scenario of *computational irreducibility* that is characteristic for some discrete dynamical systems, such as cellular automata [15]. Fortunately, for solitons it has been the overwhelming experience that the opposite is true: there is a surprisingly large *reducibility*. Namely, a deep understanding of the dynamics seems to be possible through tracking only a few effective degrees of freedom, called *collective coordinates* (CCs).

This is most evident for multi-soliton configurations that are Bogomolny–Prasad–Sommerfield (BPS) [16,17]. The small-velocity scattering of BPS solitons can be accurately described using the moduli (geodetic) approximation, where the CCs are time-dependent parameters (moduli) of the static solution, such as mutual separations, etc. Integrating the field's kinetic energy for this background we get a metric of the moduli space, a curved manifold of BPS solutions, and the scattering of solitons is equivalent to geodetic motion [18].

For a non-BPS case, the canonical moduli space does not exist and we are forced to guess. However, a general strategy, which can be perhaps called an *adiabatic* method, uses the same principle, namely it introduces an ad hoc moduli space that aspires to capture the dynamics under investigation. The coordinates of this space become dynamical variables in the resulting collective coordinate model (CCM), usually resembling the classical mechanics of interacting point masses.

In the case of ϕ^4 kinks, there are no static multi-kink solutions (however, one can stabilize them by adding impurities [12]). The use of CCM for ϕ^4 kinks has a long, fruitful, and somewhat complicated history (see Ref. [14] for a recent overview). For our purposes, let us highlight two important results.

First, for a single kink, it was noticed a long time ago [19] that a correct CCM (in the sense of both qualitative and quantitative agreement) must include not only the position modulus but also a scaling modulus. If we plug the ansatz

$$\phi_{\text{bkg}} = \tanh\big(b(t)(x - a(t))\big) \tag{1}$$

into the Lagrangian and integrate over x, the resulting effective theory (Eq. (48)), while non-linear, can be exactly integrated and contain both a Lorentz-boosted kink solution and exact harmonic motion, intimately connected with the so-called *Derrick mode* of the kink [10]. This mode has been recognized as a key tool for recovering the Lorentz covariance that is typically lost in CCMs.

The second result is the recent identification of quantitatively correct CCM for $K\bar{K}$ scattering [10,11,13] that is based on the observation that a simple $K\bar{K}$ superposition ansatz,

$$\phi_{\text{bkg}} = \tanh\big(b(t)(x + a(t))\big) - \tanh\big(b(t)(x - a(t))\big) - 1, \tag{2}$$

leads to a moduli space with an unremovable singularity at the point $a = 0$. Therefore, in Ref. [13] the authors proposed a perturbative approach for incorporating the scaling modulus order by order. The resulting CCMs do not suffer from the singularity at $a = 0$ and seem to qualitatively and quantitatively match observed $K\bar{K}$ dynamics.

The use of CCMs is, of course, not limited just to $K\bar{K}$ scattering, but can also be applied to other problems, such as the lifetime of an oscillon. A field-theoretical oscillon is a meta-stable state that is observed in the collapse of bubbles, usually taken as Gaussian peaks placed on top of a vacuum. Compared with models with only a single vacuum, when the scalar field theory has two or more vacua, the lifetime of such bubbles is typically much longer than one would

naively expect. Further, certain universal features are shared across various initial conditions and models. At the onset, the initial profile quickly settles to a certain shape around which it oscillates quasi-periodically for a long time, slowly radiating away energy, until it suddenly decays. Oscillons enjoy a long history of investigation, although typically in spatial dimensions higher than one [20–27].

It is easy to construct a simple CCM for an oscillon that captures some of its key properties. In ϕ^4 theory, if we use the background

$$\phi_{\mathrm{bkg}} = -1 + A(t)e^{-x^2/R(t)^2}, \tag{3}$$

we get the effective Lagrangian

$$\sqrt{\frac{2}{\pi}}L_{\mathrm{osc}} = \frac{1}{2}R\dot{A}^2 + \frac{1}{2}A\dot{A}\dot{R} + \frac{3\dot{R}^2A^2}{8R} - \frac{A^2}{2R} - 2A^2R + 2\sqrt{\frac{2}{3}}A^3R - \frac{A^4R}{2\sqrt{2}}. \tag{4}$$

Numerical investigations of this CCM[1] reveal that for most initial values there exists, after a short initial phase, a long quasi-periodic regime after which the "bubble" collapses exponentially fast ($A \to 0$ and $R \to \infty$). In that regard, the above CCM is qualitatively faithful to what is going on in field theory, at least for small energies. For energies large enough, we can expect that the oscillon decays into a $K\bar{K}$ pair (that can also undergo a few bounces before separation) as Fig. 1 illustrates.

This behavior is, of course, impossible to predict using Eq. (4), which is inadequate for any situations where the field significantly departs from the Gaussian shape. Of course, one can attempt to remedy this by introducing more complicated ansatzes.

Concrete CCMs will have limited applicability specific to a given situation. However, there are also general limitations. The most apparent one is pragmatic. Typically, when the number of collective coordinates exceeds $N = 2$, the resulting formulae algebraically explode. Indeed, it is hard to come up with an N-dimensional moduli space for which the effective Lagrangian can be written down in a closed (and manageable) form. We can see that for $K\bar{K}$ scattering CCMs that include either normal modes [14] or higher Derrick modes [13]. Simply put, N-point CCMs are typically *algebraically intractable*.

This leads to a closely related limitation, namely that CCMs are usually not introduced as members of a perturbative schema that approaches the full configuration space in a limit. In other words, CCMs are not usually *exhaustive*. Having constructed one CCM, however successful, it is not a priori clear how to make the next step that would further deepen our understanding. In other words, typical CCMs are isolated islands of limited applicability that have no relation to one another.

Of course, this aspect might be both a strength and a weakness of the adiabatic approach. We can use it to zoom in on a particular aspect of the theory, such as $K\bar{K}$ scattering, and ignore everything else. By construction, a CCM reflects our *a priori* knowledge about the solution space. Thus, it is difficult to be surprised, and we cannot use CCMs to discover completely new phenomena.[2]

In contrast, in this paper we present a general-purpose CCM which attempts to overcome the aforementioned limitations. The three criteria that we demand are (i) *algebraic tractability* for an N-point CCM, (ii) *exhaustiveness*, e.g. that the CCM approaches the field theory as

---

[1]See Sect. 4, where we study essentially the same model.

[2]Let us, however, point out that the spectral wall phenomenon [28] might be a good counterexample for this generalizing statement.
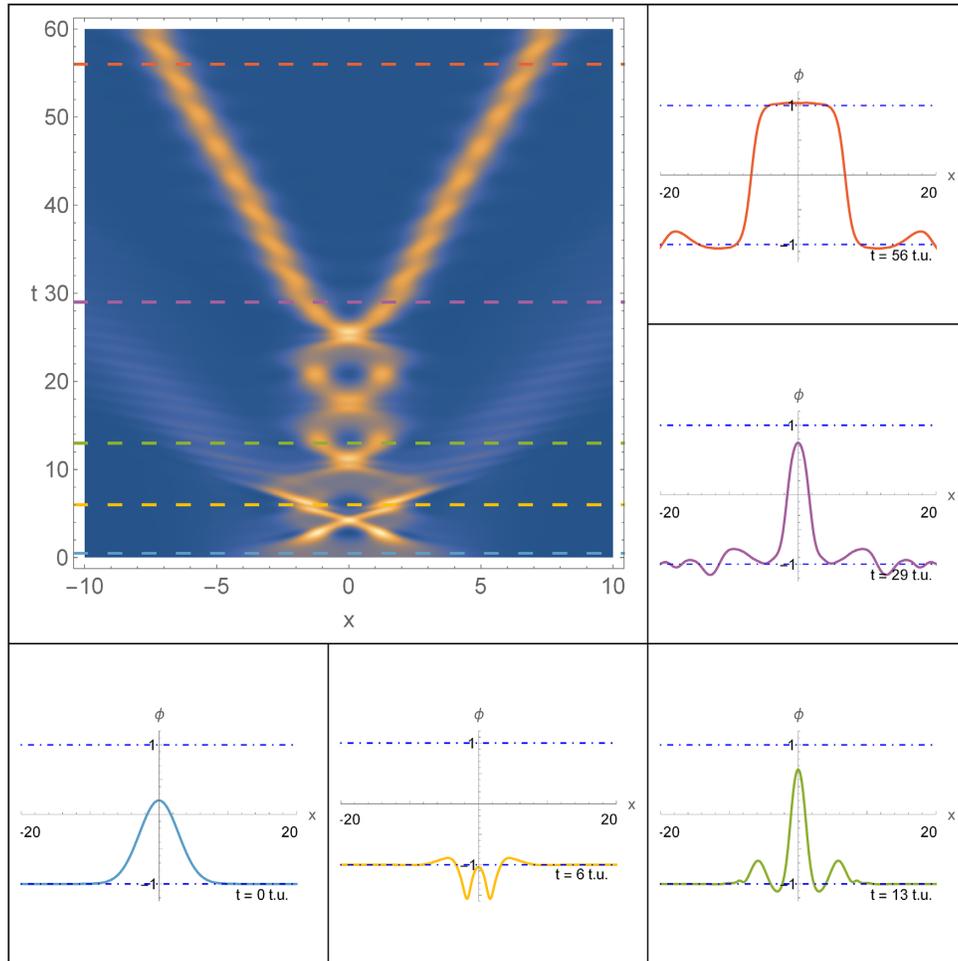
Fig. 1. Plot of the energy density and field profiles for several timestamps in the ϕ^4 model, showcasing a disintegration of a Gaussian peak into a kink–anti-kink pair.

$N \to \infty$, and (iii) *qualitative* agreement between dynamical phenomena. Note that we do not (yet) demand *quantitative* agreement, but rather regard it as an ultimate test.

In particular, we present the *simplest* (that we can imagine) general-purpose CCM that passes these criteria. However, we do not claim that it is also an optimal approach; indeed, there are deficiencies that we will point out. We regard our construction as a proof of concept.

We call our approach *mechanization*. We replace a smooth field $\phi(x, t)$ by piecewise linear segments, i.e. a linear graph with a given number of "joints" (vertices) connected with straight "segments" (edges). The positions of joints and the associated field values (populations on the graph) are the time-dependent CCs. In other words, the continuous field, upon mechanization, becomes a jagged line resembling an axle connecting wheels on a steam train (see Fig. 2).

Despite its conceptual simplicity, mechanization is surprisingly successful in capturing essential phenomena of scalar field theories, such as bouncing and bion pair-production in $K\bar{K}$ scattering. As it does not require any prior knowledge, we can in fact *discover* these phenomena by gradual exploration of "mech-models." Indeed, the first two smallest values of N reveal the mech-kink solution (a mechanical analog of a field-theoretical kink) and the mech-oscillon (an analog of the oscillon) with the same CCMs as those in Ref. [19] and Eq. (4) without any prior insight. Furthermore, the bouncing phenomenon, bion pair-production, as well as more
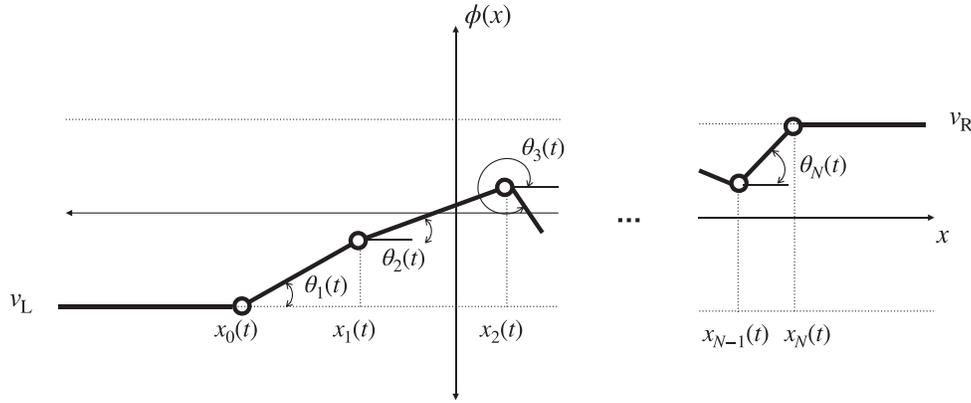
Fig. 2. A depiction of a mech-field $\phi_M(x, t)$ as a sequence of N straight segments connected via free-moving joints.

intricate patterns can be easily spotted in decay states of higher-N mech-oscillons. As these "mech-phenomena" gradually appear in an ordered sequence in complexity, we can use mechanization as a tool for *systematic* exploration of a scalar field theory.

The requirement for algebraic tractability is essential to this feature. As we will show, mechanization yields compact formulae for an arbitrary number of joints. In particular, we can write down the effective Lagrangian, the equations of motion, and the metric for N joints explicitly.

In Sect. 2 we describe the mechanization method, the effective Lagrangian, its symmetries, and the metric. In Sect. 3 we investigate mech-models with topological boundary conditions, mech-kinks, while in Sect. 4 we turn our attention to topologically trivial configurations, mech-oscillons. Lastly, in Sect. 5 we summarize our findings and discuss limitations and possible improvements.

2. Mechanization

2.1 Mech-field

Mechanization is simply a replacement of a continuous field $\phi(x, t)$ with a piecewise linear function which we dub a *mech-field* $\phi_M(x, t)$. We express it mathematically as[3]

$$\phi(x, t) \underset{M}{\to} \phi_M(x, t) \equiv \sum_{a=-1}^{N} \big(k_{a+1}(t)(x - x_a(t)) + \phi_a(t)\big)\chi_a, \tag{5}$$

where $x_a(t)$ are the positions of $N + 1$ joints, $\phi_a(t) \equiv \phi(x_a(t))$ are the field values, and

$$k_{a+1} \equiv \frac{\Delta\phi_a}{\Delta x_a} = \frac{\phi_{a+1} - \phi_a}{x_{a+1} - x_a} = \tan\big(\theta_a(t)\big) \tag{6}$$

are the slopes of ath segments (see Fig. 2). For our definition of mech-field to work, we formally assign joints to both spatial infinities, namely $x_{-1} = -\infty$ and $x_{N+1} = +\infty$. Furthermore, we always assume that the outermost segments are horizontal and lie in some vacua, i.e. $k_0 = k_{N+1} = 0$ and $\phi_{-1} = \phi_0 = v_L$, $\phi_N = \phi_{N+1} = v_R$, where $v_{L(R)}$ are left (right) vacuum values. Also, the positions of segments form an ordered sequence $x_0(t) \leq x_1(t) \leq \cdots \leq x_N(t)$.

The χ_a are the indicator functions for each segment, namely $\chi_a = 1$ inside the interval (x_a, x_{a+1}) and zero outside:

$$\chi_a \equiv \theta(x - x_a) - \theta(x - x_{a+1}) = -\Delta\theta(x - x_a), \tag{7}$$

---

[3]We use the symbol $\underset{M}{\to}$ to indicate the mechanization of a continuous variable.

where the Heaviside step function is defined by

$$\theta(x) = \lim_{\varepsilon \to 0^+} \int_{-\infty}^{\infty} \frac{d\omega}{2\pi i} \frac{e^{i\omega x}}{\omega - i\varepsilon} = \begin{cases} 1 & \text{if } x > 0, \\ 0 & \text{if } x < 0. \end{cases} \tag{8}$$

The value $\theta(0)$ is left unspecified, but it has no impact on the physics.

In a certain sense, it might seem that there are too many variables. A standard way of discretizing space would be to replace a continuum variable x with a lattice, or in general with a fixed grid. In contrast, in our approach, the grid is itself dynamic. A dynamic grid is often employed to improve the precision of the numerical integration of differential equations. There, however, the choice of grid spacing is dictated by optimization, while in our case the dynamics originate by construction.

2.2 *From mech-field to field*

It is easy to imagine a formal limit that gives us back the original continuous field variable $\phi(x, t)$. If we send $N \to \infty$ in such a way that the joints become dense on the entire x-axis, i.e. $x_a(t) \to \xi$, the summation becomes an integration:

$$\phi_M(x, t) = \sum_{a=-1}^{N} \big(k_{a+1}(t)(x - x_a(t)) + \phi_a(t)\big)\chi_a$$

$$\times \xrightarrow[N \to \infty]{\int} \int_{-\infty}^{\infty} d\xi \, \big(\phi'(\xi)(x - \xi) + \phi(\xi)\big)\delta(x - \xi) = \phi(x), \tag{9}$$

where we used the following correspondence: $k_{a+1} \to \phi'(\xi)$ and $\chi_a \to \delta(x - \xi)d\xi$ as $N \to \infty$.

Even without taking the continuous limit, we can directly relate the discrete variables $\{x_a(t), \phi_a(t)\}$ and the time-dependent Fourier coefficients of $\phi(x, t)$ through Eq. (8). In particular, after some algebra, we have

$$\phi(x, t) \xrightarrow[M]{} \frac{1}{2} \int_{-\infty}^{\infty} \frac{d\omega}{2\pi} \big(Y(\omega)e^{i\omega x} + Y^*(\omega)e^{-i\omega x}\big) + \frac{v_L + v_R}{2}, \tag{10}$$

where

$$Y(\omega) \equiv -\frac{1}{\omega^2} \sum_a \Delta k_a(t)e^{-i\omega x_a(t)}. \tag{11}$$

Notice that $Y(\omega)$ are nothing but the Fourier coefficients of the mech-field $\phi_M(x, t) - v_L$, while $Y^*(\omega)$ are the Fourier coefficients of $\phi_M(x, t) - v_R$.

It is worth mentioning that one can assign a set of $2N$ discrete variables $\{x_a(t), \phi_a(t)\}$ to a given function $\phi(x, t)$. This can be achieved by expanding $Y(\omega)$ as a Taylor series in ω up to the $2N$th power and matching the result with equivalent series for the Fourier image of $\phi(x, t) - v_L$. From this point of view, mechanization can be roughly understood as an attempt to faithfully represent small frequencies (long wavelengths) using the most simple functions available: piecewise linear functions.

2.3 *Effective Lagrangian*

We derive the effective Lagrangian by plugging Eq. (5) into a canonical Lagrangian for a single scalar field,

$$\mathcal{L} = \frac{1}{2}\dot{\phi}^2 - \frac{1}{2}\phi'^2 - V(\phi), \tag{12}$$

where the potential has two degenerate minima, v_L and v_R, i.e. $V(v_{L,R}) = V'(v_{L,R}) = 0$.

The integration procedure is straightforward and yields compact formulas. Let us illustrate it on $\phi'^2_M/2$. If we adopt the derivative ϕ'_M as a differential consequence of Eq. (5),

$$\phi'(x, t) \underset{M}{\to} \sum_{a=-1}^{N} k_{a+1} \chi_a \equiv \phi'_M(x, t), \tag{13}$$

it follows that

$$\frac{1}{2} \int_{-\infty}^{\infty} dx\, \phi'^2 \underset{M}{\to} \frac{1}{2} \sum_{a,b} k_{a+1} k_{b+1} \int_{-\infty}^{\infty} dx\, \chi_a \chi_b = \frac{1}{2} \sum_{a=0}^{N-1} k_{a+1}^2 (x_{a+1} - x_a), \tag{14}$$

where we have used the obvious identity $\chi_a \chi_b = \chi_a \delta_{ab}$. Notice that the resulting formula only involves the coupling of neighboring joints, and it is also manifestly positive (as $x_{a+1} \geq x_a$ by definition).

Similarly, we calculate the kinetic energy,

$$\frac{1}{2} \int_{-\infty}^{\infty} dx\, \dot{\phi}^2 \underset{M}{\to} \frac{1}{6} \sum_{a=-1}^{N} \Delta x_a \left(\Phi_{a+1,a}^2 + \Phi_{a+1,a} \Phi_{a,a} + \Phi_{a,a}^2 \right),$$

where we write $\Phi_{a,b} \equiv \dot{\phi}_a - k_{b+1} \dot{x}_a$ for convenience. The above expression can be recast in manifestly positive form as

$$\frac{1}{2} \int_{-\infty}^{\infty} dx\, \dot{\phi}^2 \underset{M}{\to} \frac{1}{12} \sum_{a=0}^{N-1} \Delta x_a \left((\Phi_{a+1,a} + \Phi_{a,a})^2 + \Phi_{a+1,a}^2 + \Phi_{a,a}^2 \right), \tag{15}$$

while the most compact explicit formula reads

$$\frac{1}{2} \int_{-\infty}^{\infty} dx\, \dot{\phi}^2 \underset{M}{\to} \frac{1}{6} \sum_{a=0}^{N-1} \dot{k}_{a+1}^2 (\Delta x_a)^3 + \frac{1}{2} \sum_{a=0}^{N-1} \Delta x_a (\dot{\phi}_{a+1} - k_{a+1} \dot{x}_{a+1})(\dot{\phi}_a - k_{a+1} \dot{x}_a). \tag{16}$$

Lastly, the potential energy is calculated as:

$$\int_{-\infty}^{\infty} dx\, V(\phi) \underset{M}{\to} \int_{-\infty}^{\infty} dx\, V\left(\sum_{a=-1}^{N} (k_{a+1}(x - x_a) + \phi_a) \chi_a \right) = \sum_{a=-1}^{N} \int_{x_a}^{x_{a+1}} dx\, V\left(k_{a+1}(x - x_a) + \phi_a \right)$$

$$= \sum_{a=-1}^{N} \frac{1}{k_{a+1}} \int_{\phi_a}^{\phi_{a+1}} d\xi\, V(\xi) = \sum_{a=0}^{N-1} \Delta x_a \frac{\mathcal{V}(\phi_{a+1}) - \mathcal{V}(\phi_a)}{\phi_{a+1} - \phi_a}, \tag{17}$$

where $\mathcal{V}$ is the primitive function of V. Notice that this is, indeed, positive: $\mathcal{V}$ is an increasing function and hence $\mathcal{V}(\phi_{a+1}) - \mathcal{V}(\phi_a)$ will be either positive or negative if $\phi_{a+1} - \phi_a$ is positive or negative.

Combining all our results, we can write the "mech-Lagrangian" compactly as

$$\int_{-\infty}^{\infty} dx\, \mathcal{L} \underset{M}{\to} L_M,$$

$$L_M = \sum_{a=0}^{N-1} \Delta x_a \left[\frac{1}{6} \left(\Delta \dot{\phi}_a - \frac{\Delta \dot{x}_a}{\Delta x_a} \Delta \phi_a \right)^2 - \frac{\Delta \phi_a^2}{2 \Delta x_a^2} + \frac{1}{2} \left(\dot{\phi}_{a+1} - \frac{\Delta \phi_a}{\Delta x_a} \dot{x}_{a+1} \right) \right.$$

$$\left. \times \left(\dot{\phi}_a - \frac{\Delta \phi_a}{\Delta x_a} \dot{x}_a \right) - \frac{\Delta \mathcal{V}(\phi_a)}{\Delta \phi_a} \right]. \tag{18}$$

2.4 *Symmetries*

Let us consider the relation between symmetries of the field theory in Eq. (12) and the mech-model in Eq. (18).

First, the conserved quantities related to translational invariance of spacetime, i.e. $x^\mu \to x^\mu + a^\mu$—energy and momentum—are preserved under mechanization. If we mechanize the continuous formulae we obtain the discrete momentum

$$P = -\int_{-\infty}^{\infty} dx\, \dot\phi \phi' \xrightarrow[\text{M}]{} \sum_{a=0}^{N-1} \Delta\phi_a \bar U_a \equiv \sum_{a=0}^{N-1} P_a \equiv P_{\text{M}} \tag{19}$$

and the discrete energy

$$E = \int_{-\infty}^{\infty} dx \left(\frac{1}{2}\dot\phi^2 + \frac{1}{2}\phi'^2 + V(\phi) \right)$$

$$\xrightarrow[\text{M}]{} \sum_{a=0}^{N-1} \left(\frac{1}{24}\dot k_{a+1}^2 (\Delta x_a)^3 + \frac{1}{2}\bar U_a^2 \Delta x_a + \frac{1}{2}k_{a+1}^2 \Delta x_a + \Delta x_a \frac{\mathcal{V}(\phi_{a+1}) - \mathcal{V}(\phi_a)}{\phi_{a+1} - \phi_a} \right) \equiv E_{\text{M}}, \tag{20}$$

where we introduced the quantity

$$\bar U_a \equiv -\frac{1}{\Delta x_a} \int_{x_a}^{x_{a+1}} dx\, \dot\phi = -\frac{1}{2}\left(\Phi_{a+1,a} + \Phi_{a,a} \right), \tag{21}$$

which we loosely interpret as the average velocity of a segment. For future reference, let us also introduce the notion of a segment's mass, namely twice the static free energy:

$$M_a \equiv \int_{x_a}^{x_{a+1}} dx\, \phi'^2 = k_{a+1}^2 \Delta x_a. \tag{22}$$

The total mass of the mech-field is thus

$$M \equiv \sum_{a=1}^{N-1} M_a = \sum_{a=1}^{N-1} k_{a+1}^2 \Delta x_a. \tag{23}$$

As stated above, both momentum P_{M} and energy E_{M} are conserved quantities. Indeed, the Lagrangian L_{M} in Eq. (18) has a translational symmetry $x_a(t) \to x_a(t) + \alpha$, and it is also invariant under the time shift $t \to t + \alpha$. Invoking Nöther's theorem, we can compute the same expressions P_{M} and E_{M} directly from L_{M}.

Unsurprisingly, the Lorentz invariance is generally lost. It is well known that invariance under boosts leads to a conserved quantity,[4]

$$J^{01} = -tP + \int_{-\infty}^{\infty} dx\, \mathcal{E}x, \tag{24}$$

that represents the uniform motion of the center of mass. A mechanized analog of this would generally not be a constant of motion.

---

[4]This follows from the conservation law $\partial_\mu \mathcal{M}^{\mu\nu\rho} = 0$, where

$$\mathcal{M}^{\mu\nu\rho} = \mathcal{T}^{\mu\nu}x^\rho - \mathcal{T}^{\mu\rho}x^\nu,$$

with $\mathcal{T}^{\mu\nu}$ being the canonical energy–momentum tensor.

One may expect that the Galilean boost should still be a good symmetry of L_{M}. However, if we make the transformation $x_a(t) \to x_a(t) - Vt$ we find that the Lagrangian changes:

$$L_{\mathrm{M}} \to L_{\mathrm{M}} - P_{\mathrm{M}}V + \frac{1}{2}MV^2. \tag{25}$$

The problem is that the total mass M is generally not a constant of motion, and hence Galilean relativity is lost.

However, we can still relate solutions with different momenta. To do this, let us redefine the variables as

$$x_a(t) = \tilde{x}_a(t) + r(t), \tag{26}$$

where $r(t)$ is a site-independent variable proportional to the average position (imposing the condition $\sum_a \tilde{x}_a = 0$). It follows that

$$L_{\mathrm{M}}(x) = L_{\mathrm{M}}(\tilde{x}) + P_{\mathrm{M}}(\tilde{x})\dot{r} + \frac{1}{2}\dot{r}^2 M(\tilde{x}), \tag{27}$$

$$P_{\mathrm{M}}(x) = P_{\mathrm{M}}(\tilde{x}) + M(\tilde{x})\dot{r}, \tag{28}$$

where we have shown the explicit dependence on $x = \{x_a\}$ or $\tilde{x} = \{\tilde{x}_a\}$ variables. We may easily identify the equation of motion for $r(t)$ to be

$$\frac{d}{dt}\Big(M(\tilde{x})\dot{r} + P_{\mathrm{M}}(\tilde{x})\Big) = 0. \tag{29}$$

The expression in the brackets is a constant of motion, namely $P_{\mathrm{M}}(x)$. Thus, if we find a solution $\tilde{x}_a(t)$ with momentum $P_{\mathrm{M}}(\tilde{x}) \equiv \tilde{P}$, we can switch to a different solution with momentum $P_{\mathrm{M}}(x) \equiv P$ via

$$x_a(t) = \tilde{x}_a(t) + (P - \tilde{P}) \int \frac{dt}{M(\tilde{x})}, \tag{30}$$

where the second term is simply $r(t)$ integrated from its equation of motion.

Lastly, for completeness, let us display the equations of motion:

$$\Delta\left[\frac{d}{dt}\left(\frac{1}{6}(\Delta x_a)^2 \dot{k}_{a+1}^2 - \frac{1}{2}\Delta\phi_a \Phi_{a+1,a} \right) + \frac{1}{6}\frac{\Delta\dot{\phi}_a^3}{\Delta\dot{\phi}_a} - \frac{1}{6}k_{a+1}^2\left(\frac{\Delta\dot{x}_a^3}{\Delta\dot{x}_a} - 3 \right) - \frac{\Delta\mathcal{V}(\phi_a)}{\Delta\phi_a} \right] = -\frac{d}{dt}P_a, \tag{31}$$

$$\Delta\left[\frac{d}{dt}\left(-\frac{1}{3}(\Delta x_a)^2 \dot{k}_{a+1} + \frac{1}{2}\Delta x_a \Phi_{a+1,a} \right) - \frac{1}{6}\left(2\Delta\dot{\phi}_a \Delta\dot{x}_a + 3\dot{x}_{a+1}\dot{\phi}_a + 3\dot{x}_a\dot{\phi}_{a+1} \right) \right.$$
$$\left. + \frac{1}{3}k_{a+1}\left(\frac{\Delta\dot{x}_a^3}{\Delta\dot{x}_a} - 3 \right) + \frac{\Delta x_a}{\Delta\phi_a}\frac{\Delta\mathcal{V}(\phi_a)}{\Delta\phi_a} \right] = \frac{d}{dt}\left(\Delta x_a \bar{U}_a \right) + V(\phi_{a+1})\Delta\frac{\Delta x_a}{\Delta\phi_a}. \tag{32}$$

Note that summation of the first line implies conservation of momentum, i.e. $\dot{P} = \sum \dot{P}_a = 0$.

2.5 Moduli space

Integrating the kinetic energy over the field where certain parameters (moduli) are promoted to time-dependent variables, i.e. $\phi(x, t; \{\mathbf{X}(t)\})$, yields a metric on the moduli space spanned by the coordinates $\{\mathbf{X}(t)\}$.

Our variables are $N + 1$ positions $\{x_a(t)\}$ and $N - 1$ field values $\{\phi_a(t)\}$ (the two outermost ones are forced to lie on vacua), i.e. $\{\mathbf{X}(t)\} \equiv \{x_a(t), \phi_a(t)\}$ giving rise to a $2N$-dimensional moduli space.

Studying the metric is especially useful for understanding the singularities of the moduli space. Given our heuristic choice of coordinates, we have no right to expect that the moduli

space will be geodetically complete. Indeed, it is not. However, unlike most N-point CCMs, we can write down our metric on the back of an envelope:[5]

$$\frac{1}{2} \int_{-\infty}^{\infty} dx\, \dot{\phi}_M^2 = \frac{1}{2} \dot{\mathbf{X}}^{\mathrm{T}} \mathbf{g}^{\mathbf{XX}} \dot{\mathbf{X}} = \frac{1}{2} \sum_{a,b=0}^{N} \left(g_{ab}^{xx} \dot{x}_a \dot{x}_b + 2 g_{ab}^{x\phi} \dot{x}_a \dot{\phi}_b + g_{ab}^{\phi\phi} \dot{\phi}_a \dot{\phi}_b \right), \qquad (33)$$

where

$$g_{aa}^{xx} = \frac{1}{3} \frac{(\Delta\phi_a)^2}{\Delta x_a} + \frac{1}{3} \frac{(\Delta\phi_{a-1})^2}{\Delta x_{a-1}}, \qquad (34)$$

$$g_{a\,a+1}^{xx} = \frac{1}{6} \frac{(\Delta\phi_a)^2}{\Delta x_a}, \quad g_{a\,a-1}^{xx} = \frac{1}{6} \frac{(\Delta\phi_{a-1})^2}{\Delta x_{a-1}}, \qquad (35)$$

$$g_{aa}^{x\phi} = -\frac{1}{3} (\phi_{a+1} - \phi_{a-1}), \quad g_{a\,a+1}^{x\phi} = -\frac{1}{6} \Delta\phi_a, \qquad (36)$$

$$g_{a\,a-1}^{x\phi} = -\frac{1}{6} \Delta\phi_{a-1}, \quad g_{aa}^{\phi\phi} = \frac{1}{3} (x_{a+1} - x_{a-1}), \qquad (37)$$

$$g_{a\,a+1}^{\phi\phi} = \frac{1}{6} \Delta x_a, \quad g_{a\,a-1}^{\phi\phi} = \frac{1}{6} \Delta x_{a-1}. \qquad (38)$$

The components g^{xx}, $g^{x\phi}$, and $g^{\phi\phi}$ are tri-diagonal due to only neighboring interactions.

There are many singularities in this metric, but it is quite straightforward to appreciate why. Most apparently, when the x-distance of neighboring joints becomes zero, i.e. $\Delta x_a = 0$, the components of g^{xx} diverge. Indeed, when $\Delta x_a = 0$ and $\phi_a \neq \phi_{a+1}$ the mech-field becomes multi-valued.[6] It is possible to remove these singularities to infinity by a change of coordinates, e.g.

$$x_a(t) = x_0(t) + \sum_{c=0}^{a} e^{b_c(t)}, \qquad (39)$$

so that $\Delta x_a = e^{b_{a+1}}$. This also enforces the ordering $x_0 < x_1 < \cdots < x_N$. We have used these coordinates in all our numerical calculations.

A more subtle issue arises when a segment becomes flat, i.e. $\Delta\phi_a = 0$. If the segment in question is not on the edges, then the metric remains well defined. In fact, g^{xx} and $g^{x\phi}$ become block-diagonal, suggesting dynamical decoupling of the left and right parts of the mech-field, in agreement with intuition. If the segment is on the border, i.e. $\Delta\phi_0 = 0$ or $\Delta\phi_N = 0$, this represents a sudden uncoupling of an edge joint. Both cases manifest an abrupt change in the mech-field, which is confirmed by looking at the formula for the determinant:

$$\left| \mathbf{g}^{\mathbf{XX}} \right| = \frac{1}{12^N} \prod_{a=0}^{N-1} \frac{(\Delta\phi_a)^4 (\Delta\phi_a \Delta x_{a+1} - \Delta\phi_{a+1} \Delta x_a)^2}{(\Delta x_a)^2}. \qquad (40)$$

As we see, the volume measure vanishes if any $\Delta\phi_a = 0$.

We can also observe that when neighboring slopes become identical, i.e. $k_a = k_{a+1}$, the determinant vanishes too. However, these instances seem to be coordinate singularities. We checked that for the first few N the expression $\sqrt{\mathbf{g}^{\mathbf{XX}}} \mathbf{R}^{\mathbf{XX}}$, where $\mathbf{R}^{\mathbf{XX}}$ is the Ricci scalar, is well defined in the limit of equal subsequent slopes.

---

[5]To avoid awkward formulae, we extend the summation ranges for ϕ coordinates, although $\dot{\phi}_0 = \dot{\phi}_N = 0$.

[6]Let us note that when $\Delta x_a \to 0$ and $\Delta\phi_a \to 0$, such that the ratio $(\Delta\phi_a)^2/\Delta x_a$ is kept fixed, the metric remains completely regular. However, this is not true for components of the Riemann tensor, which diverge.
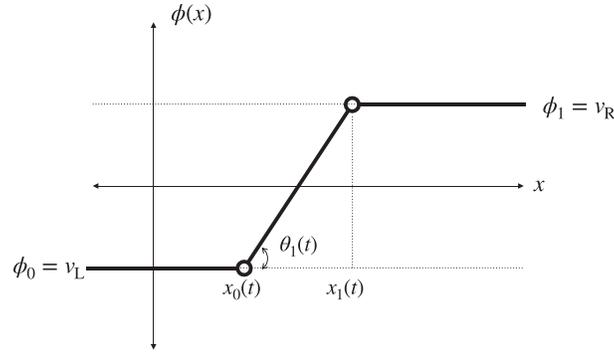
Fig. 3. Simplest mechanical model of a kink: a "mech-kink."

3. Mech-kink

In this section we begin a systematic investigation of solutions of the mech-model in Eq. (18) for increasing values of N. Here we mostly focus on static solutions of topological configurations, that we call mech-kinks. As we shall see, the model for the simplest mech-kink is totally integrable and formally equivalent to the relativistic CCM of a BPS kink [13].

3.1 $N = 1$ mech-kink

Let us consider the $N = 1$ case with topological boundary conditions, i.e. $\phi_0 = v_L \neq \phi_1 = v_R$, which we call a *mech-kink* (see Fig. 3). The Lagrangian from Eq. (18) for $N = 1$ is explicitly given by

$$L_M^{N=1} = \frac{(\Delta\phi_0)^2}{24\Delta x_0}\left((\Delta\dot{x}_0)^2 - 12 + 12\,\dot{\bar{x}}^2\right) - \kappa\,\Delta x_0, \tag{41}$$

where we have written the average position as $\bar{x} \equiv (x_0 + x_1)/2$ and the constant

$$\kappa \equiv \frac{1}{v_R - v_L}\int_{v_L}^{v_R} d\xi\, V(\xi). \tag{42}$$

The equations of motion read

$$\frac{d}{dt}\left(\frac{(\Delta\phi_0)^2 \Delta\dot{x}_0}{12\Delta x_0}\right) = -\frac{(\Delta\phi_0)^2}{24(\Delta x_0)^2}\left((\Delta\dot{x}_0)^2 - 12 + 12\,\dot{\bar{x}}^2\right) - \kappa, \tag{43}$$

$$\frac{d}{dt}\left(\frac{(\Delta\phi_0)^2 \dot{\bar{x}}}{\Delta x_0}\right) = 0. \tag{44}$$

The two conserved quantities are:

$$E_M^{N=1} = \frac{(\Delta\phi_0)^2}{24\Delta x_0}\left((\Delta\dot{x}_0)^2 + 12 + 12\,\dot{\bar{x}}^2\right) + \kappa\,\Delta x_0, \tag{45}$$

$$P_M^{N=1} = \frac{(\Delta\phi_0)^2}{\Delta x_0}\dot{\bar{x}}. \tag{46}$$

Note that $\Delta\phi_0 = v_R - v_L$ is a constant.

Let us first consider a static mech-kink: $\Delta\dot{x}_0 = \dot{\bar{x}} = 0$. Solving the equations of motion in Eqs. (43) and (44), we find the energy $E_{M,\,\text{static}}^{N=1} \equiv m_K$ and the width $R_K \equiv \Delta x_0$ to be

$$m_K = (v_R - v_L)\sqrt{2\kappa}, \qquad R_K = \frac{v_R - v_L}{\sqrt{2\kappa}}. \tag{47}$$

For concreteness, if we consider the ϕ^4 potential $V(\phi) = (1 - \phi^2)^2/2$, we have $v_R = -v_L = 1$ and $\kappa = 4/15$. The corresponding numbers for a static mech-kink read $m_K = \sqrt{32/15}$ and $R_K = \sqrt{15/2}$. Notice that the mech-kink's mass is equal to the total mass of the mech-field, i.e. $m_K = M_0 = (\Delta\phi_0)^2/\Delta x_0$.

Surprisingly, the Lagrangian $L_M^{N=1}$ is formally equivalent to a relativistic CCM for a BPS kink (Eq. (II.17) of Ref. [13]):

$$L[a, b] = \frac{1}{2}Mb\dot{a}^2 + \frac{Q}{2b^3}\dot{b}^2 - \frac{1}{2}M\left(b + \frac{1}{b}\right), \tag{48}$$

which is obtained in ϕ^4 theory using the anstaz $\phi_K = \tanh(b(x - a))$. Here, $M = 4/3$ is the kink's mass and Q is the second moment of the static kink's energy density:

$$Q = \int_{-\infty}^{\infty} dx\, x^2 \phi_K'^2(x) = \frac{\pi^2 - 6}{9}. \tag{49}$$

The similarity of Eqs. (41) and (48) becomes explicit if we set

$$\Delta x_0 = \frac{R_K}{b}, \qquad \bar{x} = a. \tag{50}$$

The Lagrangian $L_M^{N=1}$ switches to the form

$$L_M[a, b] = \frac{1}{2}m_k b\dot{a}^2 + \frac{q_M}{2b^3}\dot{b}^2 - \frac{1}{2}m_k\left(b + \frac{1}{b}\right), \tag{51}$$

where

$$q_M \equiv \int_{-\infty}^{\infty} dx\, x^2 \phi_M'^2(x) = \frac{1}{12}R_K \Delta\phi_0^2. \tag{52}$$

For the ϕ^4 model $m_K = \sqrt{32/15} \approx 1.46$, which is not far off the BPS value $4/3 \approx 1.33$. However, $q_M = \sqrt{5/6} \approx 0.91$ is more than twice the field-theoretical value $Q \approx 0.43$.

Let us stress that a priori we had no right to expect this formal correspondence. The mech-field $\phi_M^{N=1}$ is not a BPS solution of the field theory, yet we see *precisely* the same effective Lagrangian as for the BPS kink. There seems to be a certain universality of CCMs, regarding the structure of terms. Indeed, it is easy to show that the same effective Lagrangian as in Eq. (48) arises for any background $\phi = f(b(x - a))$ provided that f'^2 has finite first three moments. Thus, the key ingredient is not the shape of the solution but the inclusion of a scaling modulus. It is something of an accident that the $N = 1$ mech-field also falls into this class of backgrounds, as the scaling modulus appears as the slope of the middle segment.

Given the exact correspondence with relativistic CCM, it is not surprising that we will find the same results, namely the Lorentz covariance and the existence of a Derrick mode. However, let us stress that from the point of view of the mech-model both results are very unexpected!

Indeed, if we consider a mech-kink moving with a uniform velocity v, i.e. $\Delta\dot{x} = 0$, $\dot{\bar{x}} = v$, the equations of motion (43)–(44) can be easily solved. We find that energy $E_M^{N=1} \equiv E_K$ and width Δx_0 follow formulae for a relativistic particle:

$$E_K = \frac{m_K}{\sqrt{1 - v^2}}, \qquad \Delta x_0 = R_K\sqrt{1 - v^2} \tag{53}$$
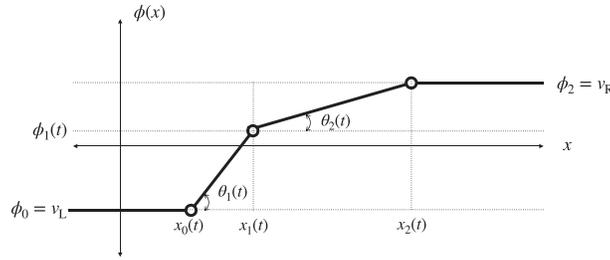
Fig. 4. Schematic depiction of an $N = 2$ mech-kink.

Let us now fix the center position to the origin $\bar{x} = 0$. If the energy E_K is above the static energy, i.e. $E_K > m_K$, the mech-kink oscillates with angular frequency $\omega_{\mathrm{M}} = \sqrt{12}/R_K$:

$$\Delta x_0 = \frac{E_K}{2\kappa} - \frac{\sqrt{E_K^2 - m_k^2}}{2\kappa} \sin(\omega_{\mathrm{M}} t). \tag{54}$$

This vibrational mode is independent of the shape of the potential. Thus, it is not a shape mode (a massive normal mode of the kink). Indeed, not all kinks have a shape mode, as is well known [6]. This mode is more appropriately identified with the so-called Derrick mode, which arises due to infinitesimal scaling of the static solution and which exists for all kinks [13]. In field theory, the frequency of the Derrick mode is $\omega_{\mathrm{D}}^2 = M/Q$. In the mech-model, it is again formally the same, $\omega_{\mathrm{M}}^2 = m_K/q_M$. Specifically, in ϕ^4 theory, $\omega_{\mathrm{M}}^2 \approx 3.1$ and $\omega_{\mathrm{D}}^2 \approx 4.4$.

We can construct a general solution of Eqs. (43) and (44) as we have the same number of unknowns, namely Δx_0 and $\bar{x}$, and constants of motion, i.e. E_K and P_K. Indeed, Eq. (44) is equivalent to $\dot{P}_K = 0$, which implies conservation of the momentum. Furthermore, Eq. (44) can be linearized as

$$\Delta\ddot{x}_0 = \frac{12 E_K}{(\Delta\phi_0)^2} - \frac{12}{(\Delta\phi_0)^2} \Delta x_0 \left(\kappa + \frac{P_K^2}{(\Delta\phi_0)^2} \right). \tag{55}$$

The general solution thus reads

$$\Delta x_0 = R_K \frac{m_K}{P_K^2 + m_K^2} \left(E_K - \sqrt{E_K^2 - P_K^2 - m_K^2} \sin\left(\frac{\sqrt{12}t\sqrt{P_K^2 + m_K^2}}{m_K R_K} \right) \right). \tag{56}$$

3.2 *N > 1 static mech-kinks*

All non-trivial static configurations are mech-kinks, by which we mean any configuration for which the outer segments lie in different vacua.[7] For instance, we depict an $N = 2$ mech-kink in Fig. 4.

The static equations of motion translate to the following conditions for the lengths of the segments:

$$\Delta x_0 = \sqrt{\frac{(\phi_1 - v_{\mathrm{L}})^3}{2(\mathcal{V}(\phi_1) - \mathcal{V}(v_{\mathrm{L}}))}}, \tag{57}$$

$$\Delta x_1 = \sqrt{\frac{(v_{\mathrm{R}} - \phi_1)^3}{2(\mathcal{V}(v_{\mathrm{R}}) - \mathcal{V}(\phi_1))}}, \tag{58}$$

---

[7]We exclude the possibility of an inner segment lying in a vacuum, as that would lead to decoupled mech-kink and anti-mech-kink solutions. These solutions nevertheless exist and can be considered as exact free mech-kink gas solutions.
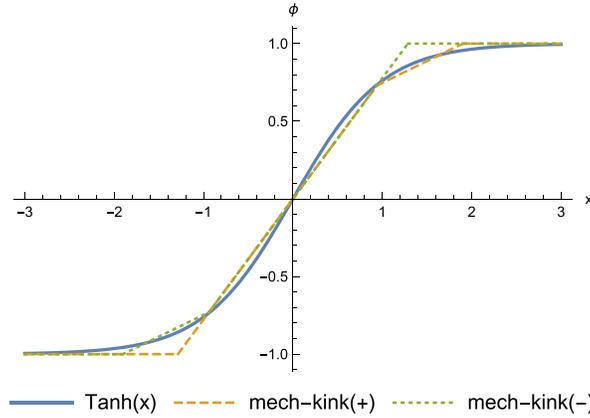
Fig. 5. Comparison between the exact kink solution in the double-well model and two static solutions for $N = 2$ mech-kinks.

while the field values satisfy the algebraic equation

$$k_0 - k_1 + V(\phi_1)\left(\frac{1}{k_0} - \frac{1}{k_1}\right) = 0, \tag{59}$$

where $k_0 = (\phi_1 - v_L)/\Delta x_0$ and $k_1 = (v_R - \phi_1)/\Delta x_1$ are the slopes of the segments. This condition can be reduced to a simpler form, namely $V(\phi_1) = k_0 k_1$, provided that $k_0 \neq k_1$. If $k_0 = k_1$ we would simply get back the $N = 1$ mech-kink solution.[8]

To be concrete, let us consider the ϕ^4 model. We found two minimum-energy solutions that are $\Delta x_0 \leftrightarrows \Delta x_1$, $\phi_1 \leftrightarrows -\phi_1$ reflections of each other (see Fig. 5):

$$\phi_1 = \frac{\pm 1}{12}\sqrt{139 - \sqrt{3865}} \approx \pm 0.73, \tag{60}$$

$$\Delta x_0 = \frac{1}{80}\left(3\sqrt{1373 + 7\sqrt{3865}} \pm \sqrt{3\left(4519 - 59\sqrt{3865}\right)}\right) \approx 1.594 \pm 0.631, \tag{61}$$

$$\Delta x_1 = \frac{1}{80}\left(3\sqrt{1373 + 7\sqrt{3865}} \mp \sqrt{3\left(4519 - 59\sqrt{3865}\right)}\right) \approx 1.594 \mp 0.631. \tag{62}$$

Their energies are the same,

$$E_{K,\pm} = \frac{1}{216}\sqrt{\frac{1}{10}(989543 - 773\sqrt{3865})} \approx 1.42 < E_K = \sqrt{\frac{32}{15}} \approx 1.46, \tag{63}$$

and are roughly 3% smaller than the energy of the $N = 1$ mech-kink. This is understandable since adding more segments should get us closer to the exact kink mass $M = 4/3 \approx 1.33$.

For $N = 3$, there is only a single minimum-energy solution, which we show in Fig. 6. Its energy is $E_K^{N=3} \approx 1.37$.

For $N = 4$, we again find two mirror-image solutions with energies $E_K^{N=4} \approx 1.36$. This pattern repeats. For odd N we get a unique solution, while for even N we find two degenerate solutions.

The static equations of motion (see Eqs. (31) and (32)) for arbitrary N reduce to

$$k_{a+1} \equiv \frac{\Delta \phi_a}{\Delta x_a} = \sqrt{\frac{2\left(\mathcal{V}(\phi_{a+1}) - \mathcal{V}(\phi_a)\right)}{\phi_{a+1} - \phi_a}}, \tag{64}$$

$$k_{a+1}k_a = 2V(\phi_a). \tag{65}$$

Notice that in the continuous limit, the first formula becomes the BPS equation for a kink, i.e. $\phi' = \sqrt{2V(\phi)}$. We can simplify the above system to a set of $N - 1$ algebraic equations for the

---

[8]This is also true for the trivial solutions $\phi_1 = v_L$ and $\phi_1 = v_R$.
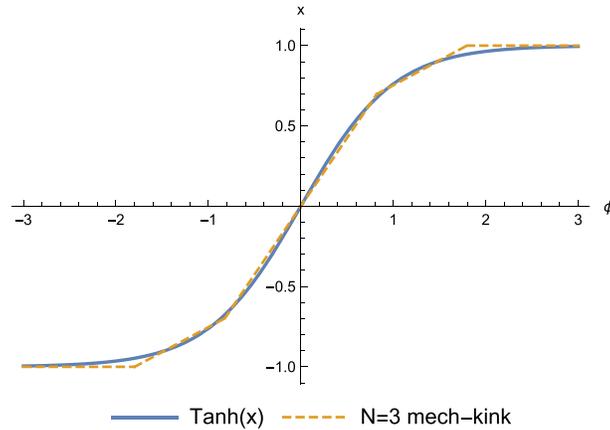
Fig. 6. Comparison between the kink solution in the double-well model and a static $N = 3$ mech-kink.

ϕ_a, namely

$$V(\phi_a) = \sqrt{\frac{\left(\mathcal{V}(\phi_{a+1}) - \mathcal{V}(\phi_a)\right)\left(\mathcal{V}(\phi_a) - \mathcal{V}(\phi_{a-1})\right)}{\left(\phi_{a+1} - \phi_a\right)\left(\phi_a - \phi_{a-1}\right)}}. \tag{66}$$

It is also easy to see that every static solution has a boosted version, meaning that the energy is equal to the static energy times the Lorentz γ factor, the field values are unchanged, while the Δx_a are contracted by $\sqrt{1 - v^2}$.

3.3 *Dynamics of mech-kinks*

There are several questions about mech-kinks that interest us but that are, however, outside the scope of this paper. For instance, we would like to know how fast the static energy approaches the BPS bound as a function of N.

Regarding the dynamics, an important query for $N \geq 2$ mech-kinks is whether there exist any exact periodic solutions. We have not been able to find the answer analytically. Numerically, however, we have glimpsed a promising candidate (see Fig. 7).

A related problem is the investigation of normal modes of the mech-kinks. In particular, we would like to study how the spectrum of small fluctuations varies with increasing N, how many spurious modes there are (compared with field theory), etc. In Fig. 8 we show a numerical solution of a slightly perturbed static $N = 2$ mech-kink indicating the presence of at least one normal mode.

Ultimately, we would like to categorize the dynamics of mech-kinks for a vast set of initial conditions to obtain a robust understanding of Cauchy's problem for each N. This task, however, is too time-consuming for our purpose here. At present, we have only sampled the evolution of a few $N \geq 2$ mech-kinks for random initial conditions via numerical integration of the equations of motion.

One phenomenon that we found to be endemic for all $N \geq 2$ mech-fields is *joint ejection*, i.e. when one of the outer joints rapidly approaches vacuum and flies either to the left or right infinity, leaving behind an effective $N - 1$ mech-field. We observe this already for $N = 2$ mech-kinks, where the left-over piece is an excited $N = 1$ mech-kink (see Fig. 9). Curiously, two joint ejections can happen simultaneously for the boundary joints, leaving behind an $N - 2$ mech-field (see Fig. 10).
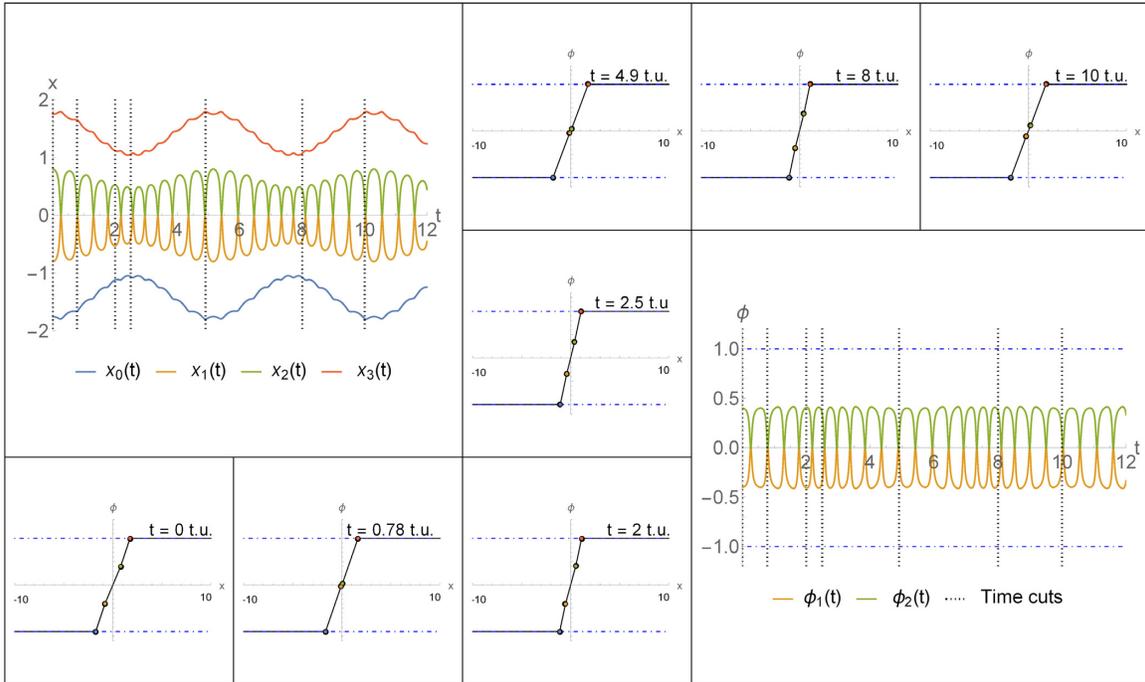
Fig. 7. Quasi-periodic oscillations in an $N = 4$ mech-kink.
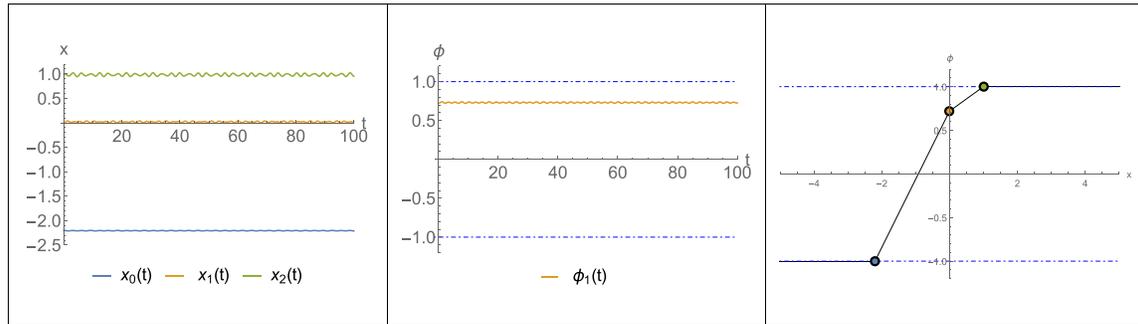
Fig. 8. Small perturbation of a static $N = 2$ mech-kink leading to quasi-periodic oscillations.

Joint ejection is indicative of a general tendency for a mech-field to simplify itself as time increases. In fact, it is not unreasonable to think that all initial configurations for mech-kinks eventually settle to an excited $N = 1$ mech-kink.

4. Mech-oscillon

In this section we investigate non-topological configurations that have $v_\mathrm{L} = v_\mathrm{R} \equiv v$. We call them generically "mech-oscillons." The simplest mech-oscillon is shown in Fig. 11.

4.1 $N = 2$: mech-field

To make the analysis as simple as possible, let us investigate a symmetric configuration, i.e. a triangle of base length $R(t)$ placed on top of the vacuum v with height $v + A(t)$ centered at the origin. In other words, we set

$$x_0(t) = -R(t)/2, \quad x_1(t) = 0, \quad x_2(t) = R(t)/2, \tag{67}$$

$$\phi_0(t) = \phi_2(t) = v, \quad \phi_1(t) = v + A(t). \tag{68}$$
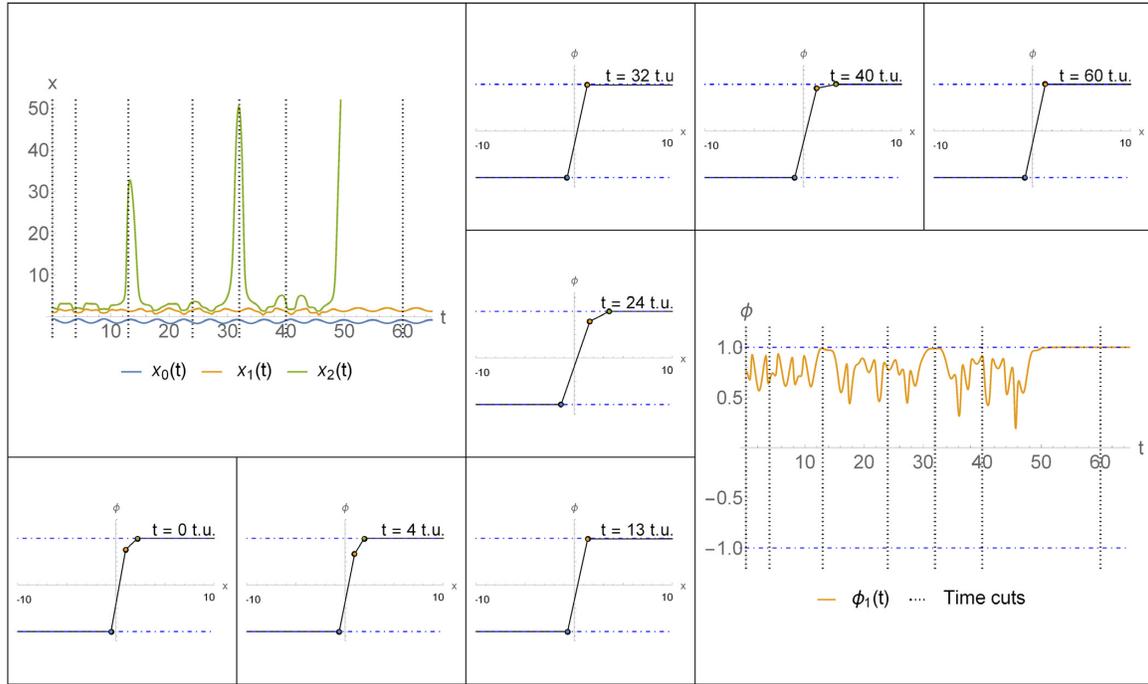
Fig. 9. An example of joint ejection for an $N = 2$ mech-kink, where the third joint escapes to ∞.
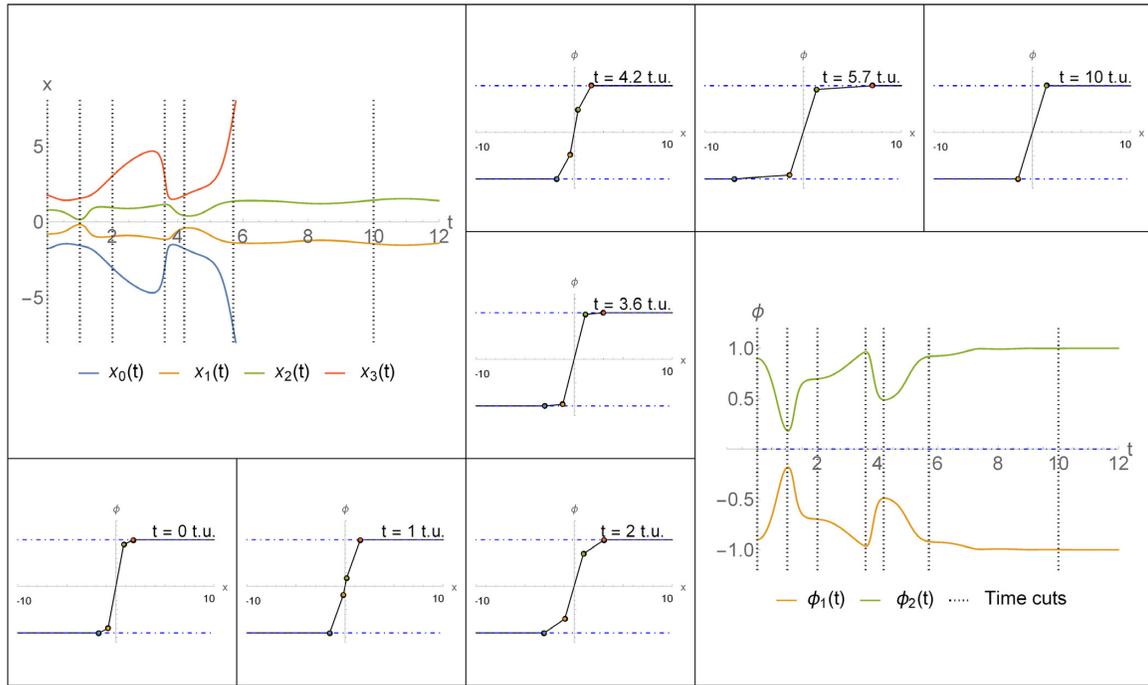
Fig. 10. A symmetric example where the outermost joints of an $N = 4$ mech-kink get ejected, leaving behind a slightly excited $N = 2$ mech-kink.

This gives us

$$L_{\mathrm{M}}^{N=2} = \frac{1}{6}R\dot{A}^2 + \frac{1}{6}A\dot{A}\dot{R} + \frac{A^2}{6R}(\dot{R}^2 - 12) - \frac{R}{A}\big(\mathcal{V}(v + A) - \mathcal{V}(v)\big). \tag{69}$$
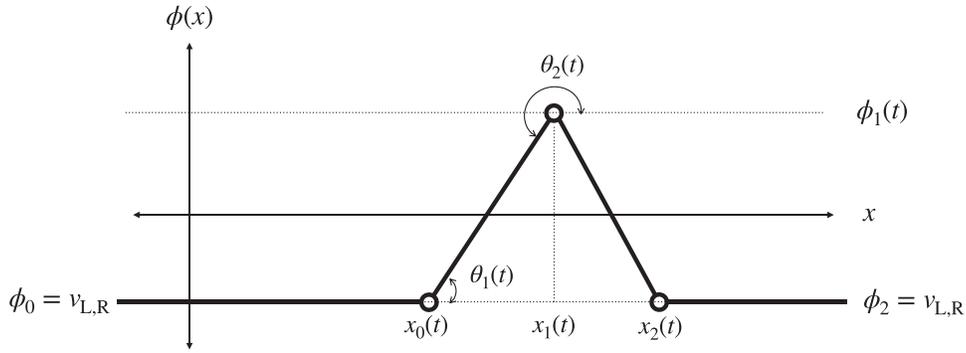
Fig. 11. Schematic depiction of $N = 2$ mech-oscillon.

In particular, for the ϕ^4 potential $V(\phi) = \frac{1}{2}\left(1 - \phi^2\right)^2$ we obtain (taking $v = -1$)

$$3L_{\mathrm{M}}^{N=2} = \frac{1}{2}R\dot{A}^2 + \frac{1}{2}A\dot{A}\dot{R} + \frac{A^2}{2R}\dot{R}^2 - \frac{6A^2}{R} - 2A^2R + \frac{3}{2}A^3R - \frac{3}{10}A^4R. \tag{70}$$

Note that $L_{\mathrm{M}}^{N=2}$ has the same structure as in Eq. (4). Again, the similarity is due to the universality of CCMs for this type of background. Indeed, it is easy to see that the same terms with varying coefficients appear when using $\phi_{\mathrm{bkg}} = -1 + Af\left(x/R\right)$, given some obvious convergence properties of f. Again, the $N = 2$ mech-kink falls into this class somewhat accidentally due to the imposed reflection symmetry. If we relax this restriction, i.e. $\Delta x_0 \neq \Delta x_1$, we no longer fit into this class, but a larger universality class of CCMs with three variables. However, we do not believe that this would yield qualitatively different dynamics.

We found it advantageous to use an exponential ansatz:[9]

$$R(t) = e^{b(t)}, \qquad A(t) = e^{a(t)}. \tag{71}$$

In these variables, the equations of motions in the ϕ^4 model read:

$$\ddot{a} = \dot{b}^2 - \dot{a}^2 + 5e^a - \frac{7}{5}e^{2a} - 20e^{-2b} - 4, \tag{72}$$

$$\ddot{b} = -2\dot{a}\dot{b} - \dot{b}^2 - e^a + \frac{2}{5}e^{2a} + 16e^{-2b}, \tag{73}$$

$$E_{\mathrm{osc}} = \frac{1}{6}e^{2a+b}\left(\dot{a}^2 + \dot{a}\dot{b} + \dot{b}^2 + 4\right) + 2e^{2a-b} + \frac{1}{10}e^{4a+b} - \frac{1}{2}e^{3a+b}, \tag{74}$$

where E_{osc} is the mech-oscillon's energy. The momentum is $P_{\mathrm{osc}} = 0$ by construction.

We plot several solutions with varying initial conditions in Figs. 12 and 13 that illustrate typical behavior of a mech-oscillon. Namely, there is an initial quasi-periodic, chaotic phase followed by a decaying phase, in which the mech-oscillon rapidly collapses to vacuum. In other words, the mech-oscillon seems to have a well-defined lifetime, whose duration is very sensitive to initial conditions. Indeed, the lifetime of a mech-oscillon can range from very short (Fig. 12) to extremely long (Fig. 13).[10] In Fig. 14, we display a "map" of the lifetime's dependence on the

---

[9]This ansatz removes the contact singularities and avoids the $\Delta\phi_0 = 0$ problem, making these coordinates especially convenient for numerical calculations. Notice that $A(t) \geq 0$ cannot go below zero. We numerically verified that, even for the general ansatz, the line $A(t) = 0$ acts as a reflective barrier if approached either from above or below; hence, our ansatz is not a loss of generality.

[10]Despite our best efforts, we did not observe the decay of this mech-oscillon. We only know that its lifetime must be longer than ~ 74000 time units. In fact, there is a common understanding that in 1+1 dimensions, oscillons can have infinite lifetimes.
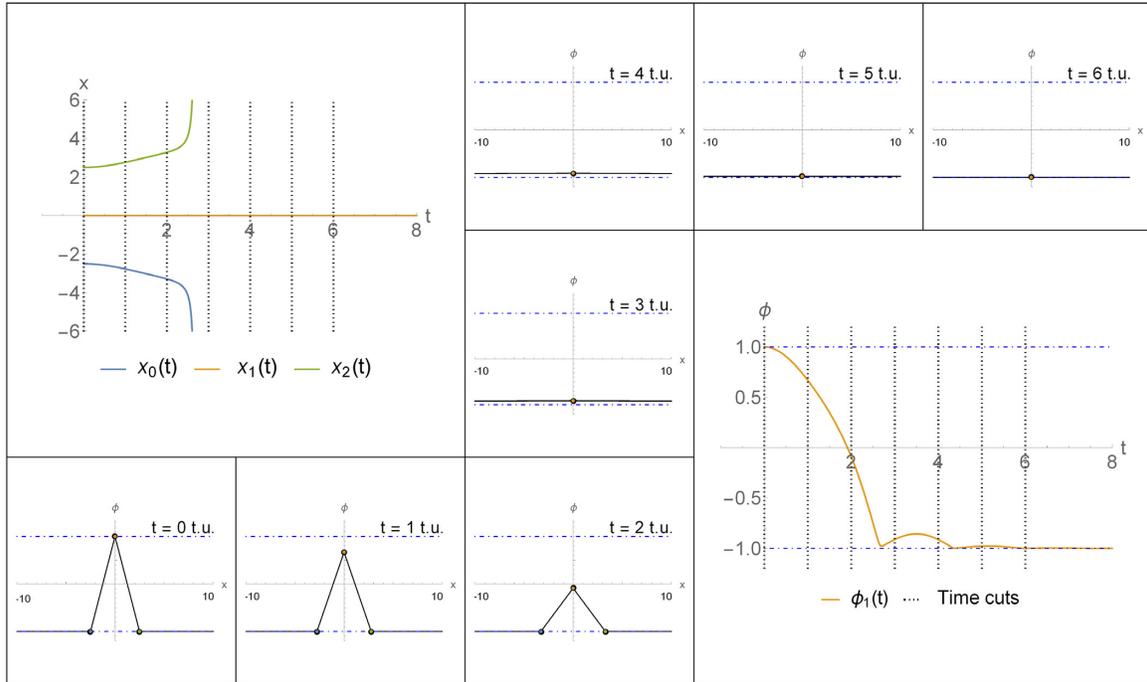
Fig. 12. Evolution of a mech-oscillon with initial conditions $R(0) = 5$ and $A(0) = 2$.
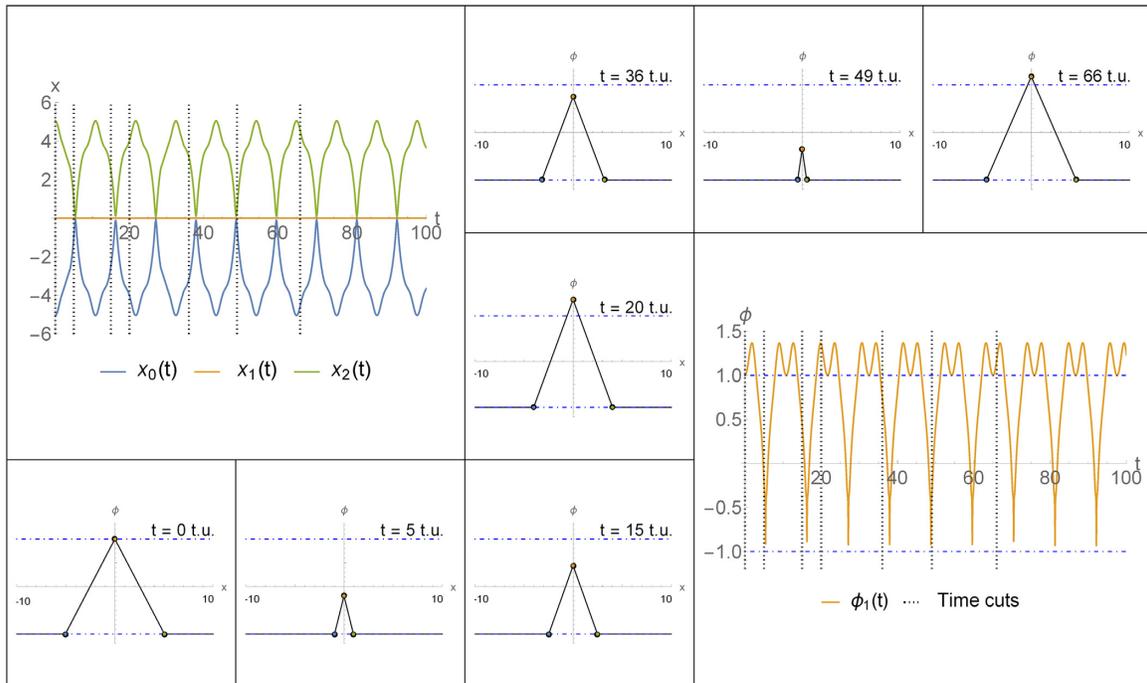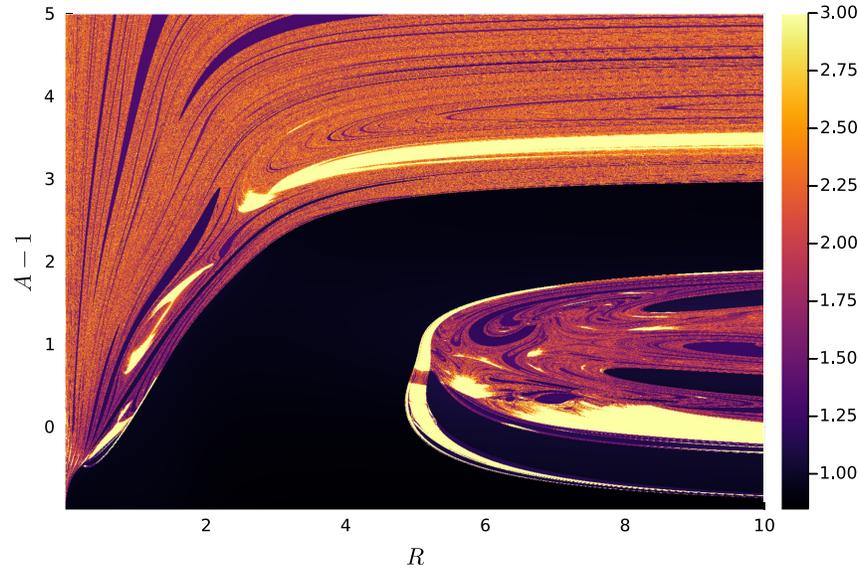

Fig. 13. Evolution of a mech-oscillon with initial conditions $R(0) = 10.1$ and $A(0) = 2$.

initial height and length of the triangle. Each color corresponds to a particular value of $\log_{10}$ of the lifetime.

Lastly, we can understand the decaying phase by studying the asymptotic properties. It is easy to show that as $t \to \infty$ we have

$$a(t) \sim -\sqrt{\frac{1}{3}V''(v)}\,t, \quad b(t) \sim 2\sqrt{\frac{1}{3}V''(v)}\,t. \tag{75}$$

19/27

Fig. 14. A "map" of the lifetimes for $N = 2$ mech-oscillons for initial values of A and R. The colors represent $\log_{10}$ of the lifetime, while lifetimes beyond 10^3 time units are all represented by the brightest color.

In other words, the height of the mech-oscillon exponentially decays, while its width exponentially grows. Also, notice that $b + 2a$ remains constant.

4.2 $N \geq 3$ mech-oscillons

Mech-oscillons display a range of behaviors for $N \geq 3$. Among others, the most significant is mech-$K\bar{K}$ pair production.

We can observe it already for $N = 3$, where the mech-$K\bar{K}$ pair immediately fly apart and de-couple from each other as the middle segment falls onto the vacuum. More interestingly, for $N \geq 4$, the created mech-$K\bar{K}$ pair remains connected via a mech-oscillon that facilitates the bouncing phenomenon (see Figs. 15 and 16). An interesting possibility suggests itself, namely a connection between the distribution of bouncing windows and the lifetime of the mech-oscillon. As far as the authors are aware, this connection has not been explored in the field theory.

It would be an interesting future project to map out the structure of the bouncing windows for $N = 4$ mech-oscillons and compare it with Fig. 14. In that way, we may confirm this connection in our mech-models. The question of whether the same can be meaningfully established in field theory, however, is subtle.

In general, a nice feature of mech-models is the gradual discovery of new behaviors as N increases. For instance, the sequential ejection of two mech-$K\bar{K}$ pairs becomes possible only at $N = 7$. For $N = 8$, we not only observe the ejection of two mech-$K\bar{K}$ pairs, but the trailing pair can also undergo a few bounces before escaping to infinity, as Figs. 17 and 18 illustrate.

A different type of behavior is the ejection of a pair of mech-oscillons, which we show in Figs. 19 and 20. In some instances (Figs. 19–21) the ejected mech-oscillons have large amplitudes that span the gap between the two vacua. These could be viewed as mech-bions, tight bound states of mech-$K\bar{K}$ pairs. In other instances (Fig. 20), the mech-oscillons have small amplitudes. More than anything else, they could represent mechanical analogs of radiative decay.

For higher N still (and sufficient energies) the mech-osillon may display a combination of all these processes. In our analysis we investigated mech-fields up to $N = 11$.
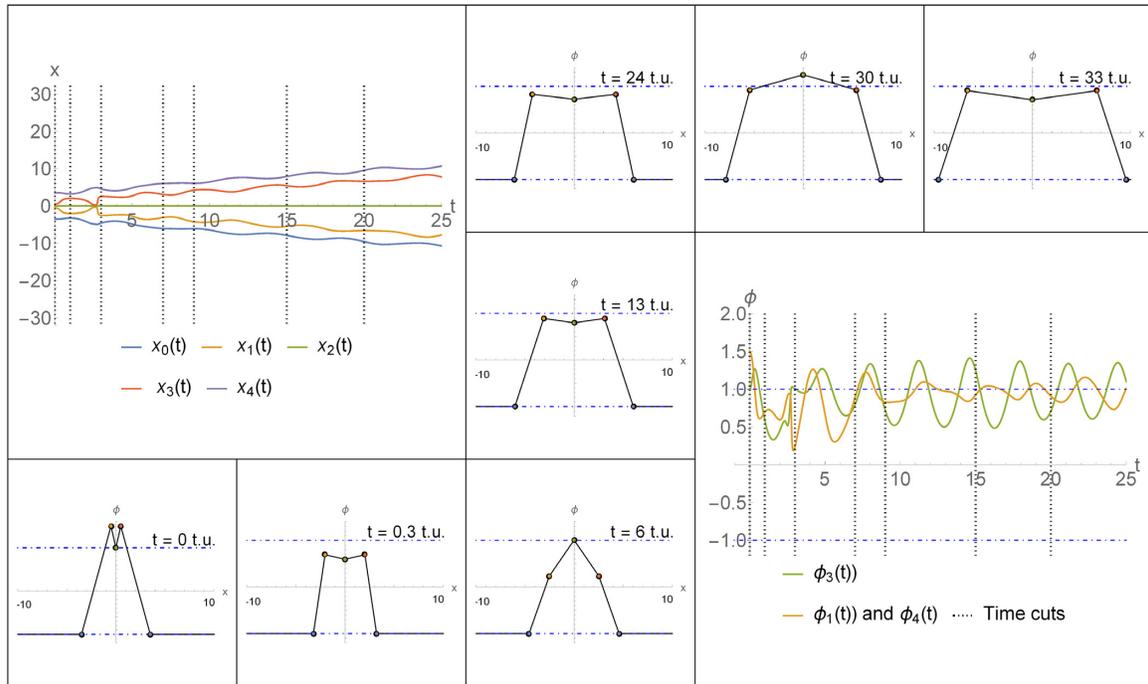
Fig. 15. A mech-$K\bar{K}$ ejection from initial $N = 4$ mech-oscillon, leaving behind an $N = 2$ mech-oscillon.
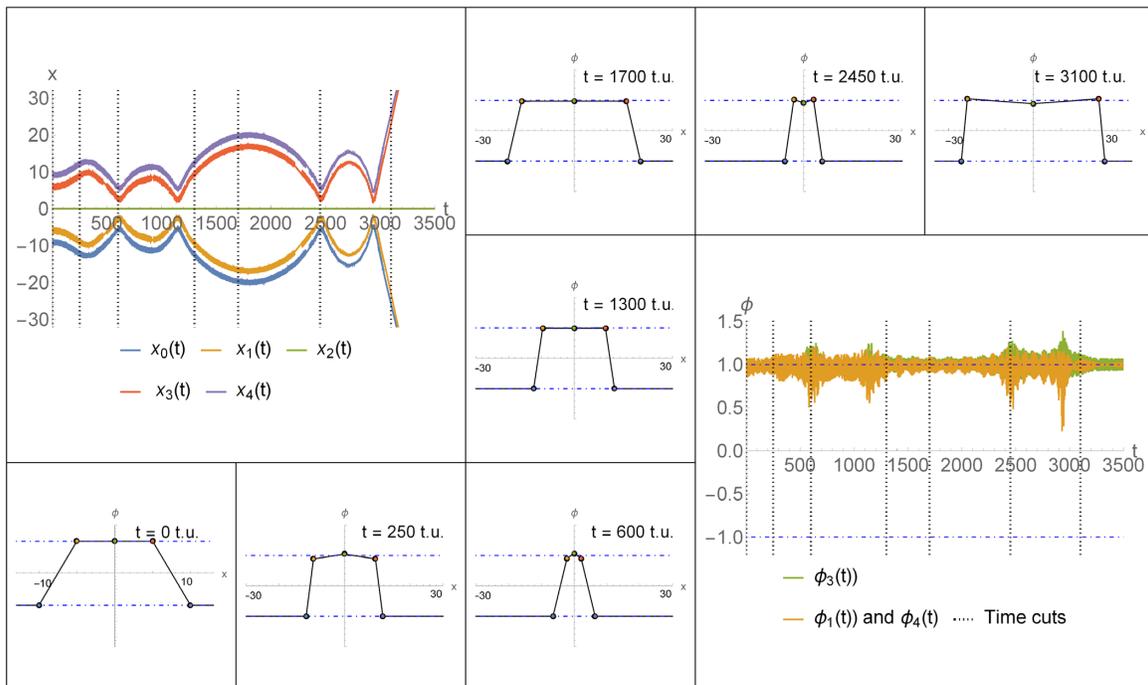

Fig. 16. Sequence of long bounces before a mech-$K\bar{K}$ ejection for an $N = 4$ mech-oscillon.

5. Summary

We have presented a general-purpose N-point CCM for a simple scalar field theory in $1 + 1$ dimensions. It is based on the "mechanization" procedure in which a continuous field is replaced by a piecewise linear function. The conceptual simplicity of our construction gave us algebraically tractable CCMs. Our numerical investigations indicate qualitative agreement between phenomena observed in mech-models and the field theory.
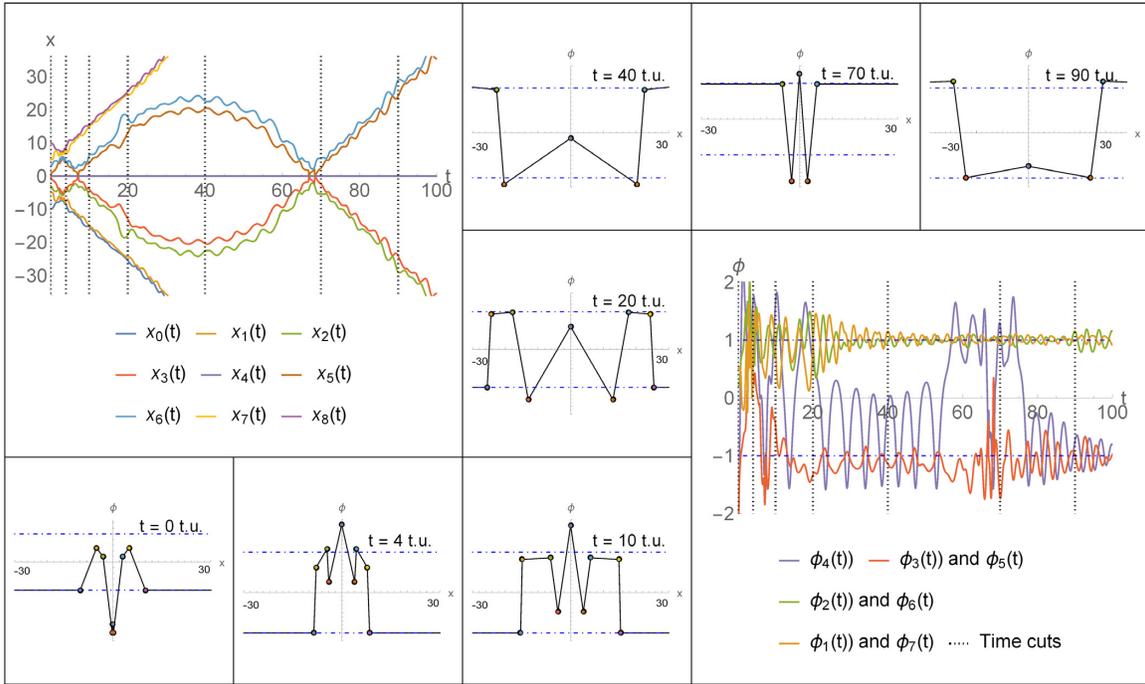
Fig. 17. Ejection of two mech-$K\bar{K}$ pairs with two intermediary bounces of the second pair for an $N = 8$ mech-oscillon.
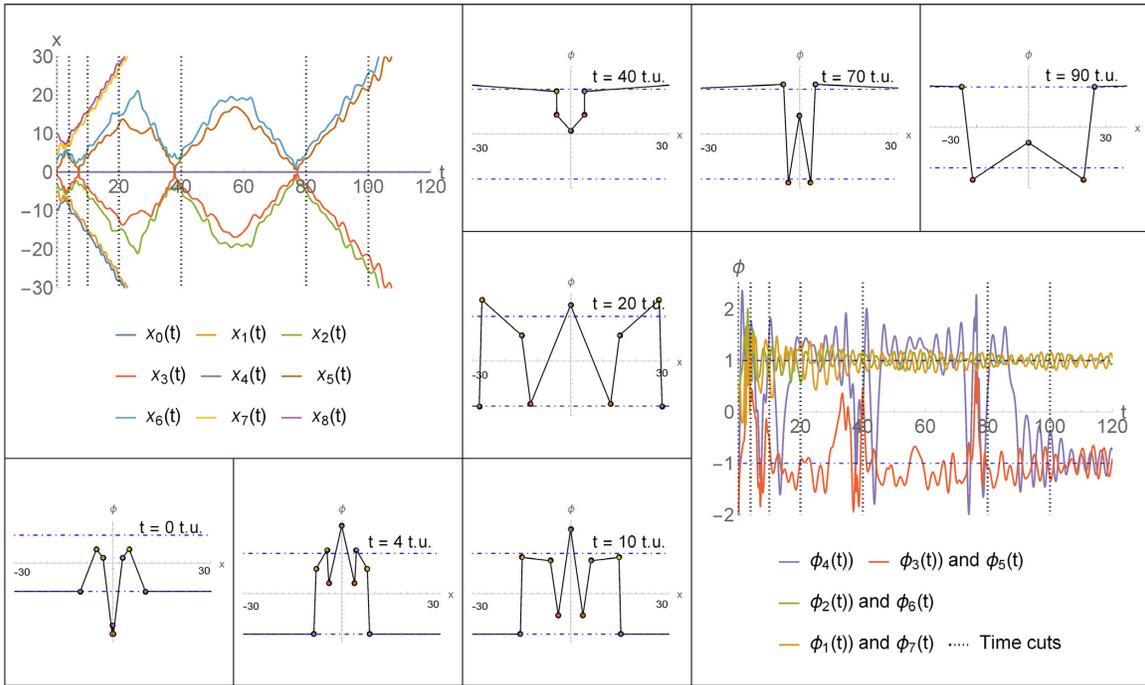
Fig. 18. Ejection of two mech-$K\bar{K}$ pairs with three intermediary bounces of the second pair for an $N = 8$ mech-oscillon.

The question of quantitative agreement is left as a future task. At this point, we may only resort to a hand-waving statement that the mech-field should resemble continuous theory more and more as N increases.
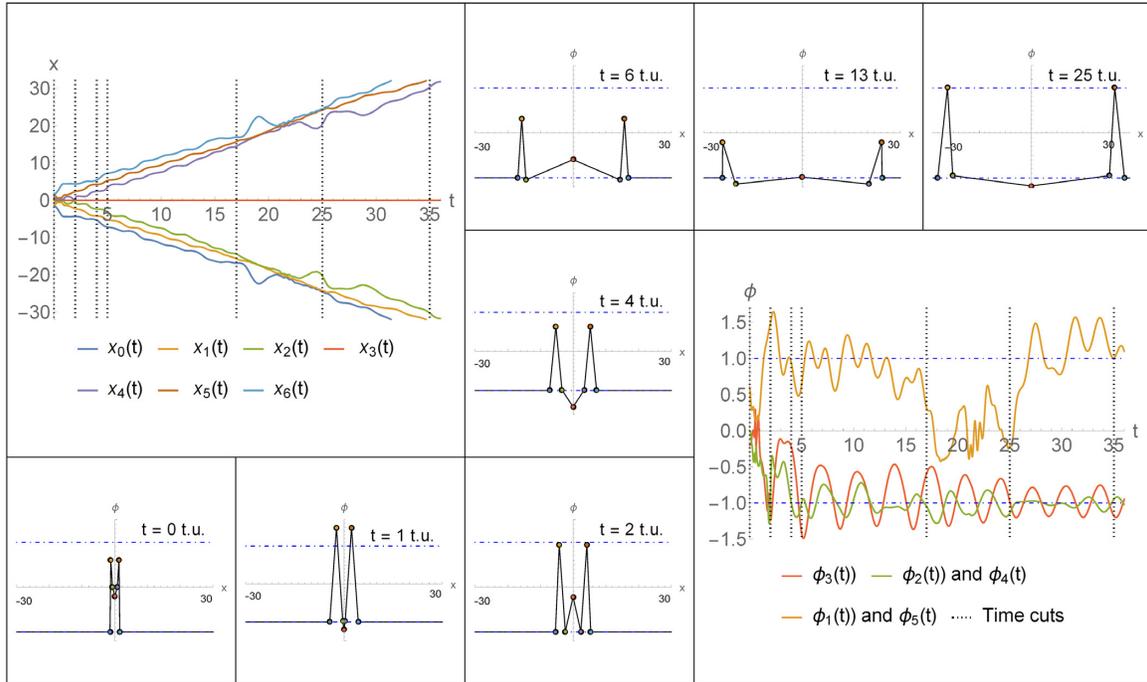
Fig. 19. Ejection of a pair of mech-oscillons for an $N = 6$ mech-field.
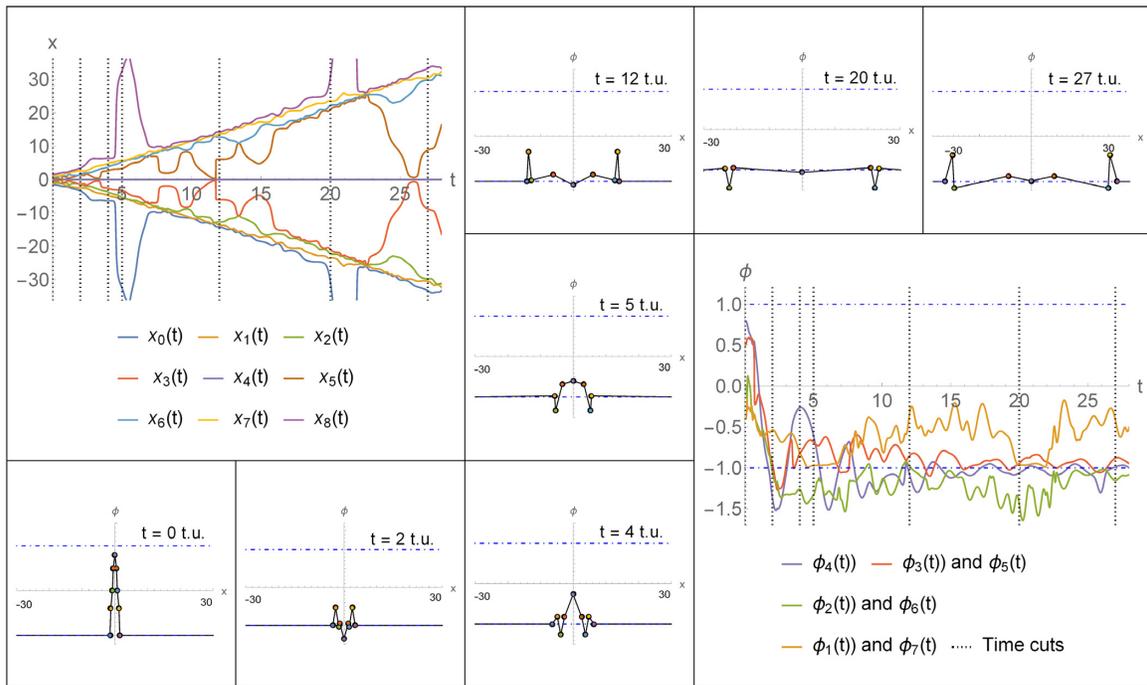
Fig. 20. Ejection of small-amplitude mech-oscillons for an $N = 8$ mech-field. Analog of radiative decay?

The most useful aspect of our approach is the natural ordering in the complexity of behaviors. As we have seen, the exploration of mech-models with an increasing number of joints gradually opens new dynamical modes of the mech-field.

Starting at $N = 1$, we have "discovered" a mech-kink that behaves as a relativistic particle. Furthermore, the corresponding mech-model in Eq. (51) turns out to be the same term-wise as
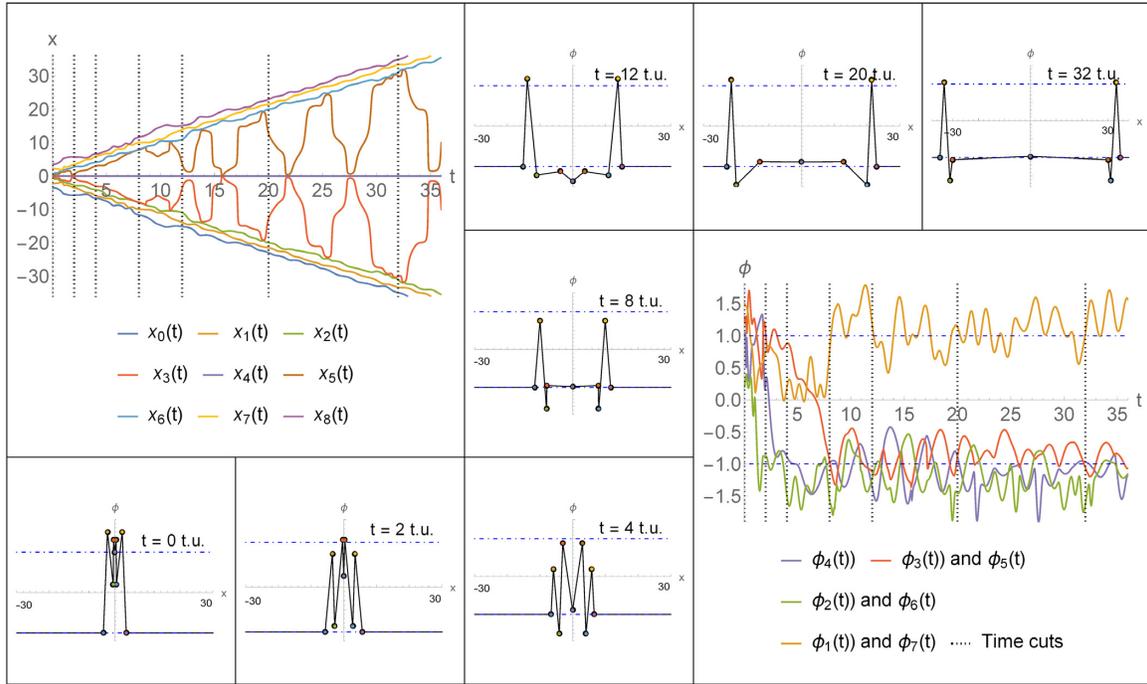
Fig. 21. Ejection of a pair of large-amplitude mech-oscillons in an $N = 8$ configuration, illustrating the production of mech-bions (tight mech-$K\bar{K}$ bound states).

relativistically covariant CCM based on the position and scaling modulus in Eq. (48). Let us point out that this result was given us *for free* without any attempt to recover the lost Lorentz covariance that motivates its construction in the field theory [10].

At $N = 2$, we have found a mech-oscillon and its tendency to suddenly decay into a vacuum after a period of time that sensitively depends on initial conditions (see Fig. 14). The corresponding CCM in Eq. (70) is, again, structurally the same as the field-theoretical one in Eq. (4).

For $N = 2$ mech-kinks, we observed a phenomenon of joint-ejection (Fig. 9) that seems to be endemic for all configurations with $N \geq 2$ (Fig. 10). The joint-ejection exemplifies a general tendency that is characteristic across our numerical data. Namely, the proclivity of an initially tightly bound mech-field to disintegrate over time into the most basic configurations, such as $N = 1$ mech-kinks and $N = 2$ mech-oscillons (or their pairs), that separate and gradually decouple from each other.

The production of mech-$K\bar{K}$ pairs can be seen already at the $N = 3$ level, but it is for $N = 4$ mech-oscillons that the phenomenon of bouncing starts to manifest (Figs. 15, 16, and 22). As the mech-$K\bar{K}$ pair is bound together via a mech-oscillon, a curious connection between the bouncing phenomenon and the mech-oscillon's lifetime suggests itself. We have not investigated this possibility in detail, however; it remains interesting future work.

At $N = 6$, yet another mode opens up, namely the ejection of a pair of mech-oscillons (Fig. 19). For $N = 8$, we observed that the peaks of ejected mech-oscillons sometimes reach all the way to the second vacuum (Fig. 21). In such situations, it seems reasonable to view the ejecta as mech-bions—tight mech-$K\bar{K}$ bound states. At other times, however, the mech-oscillons have very small amplitudes. These situations are perhaps analogs of field-theoretical radiation decay.
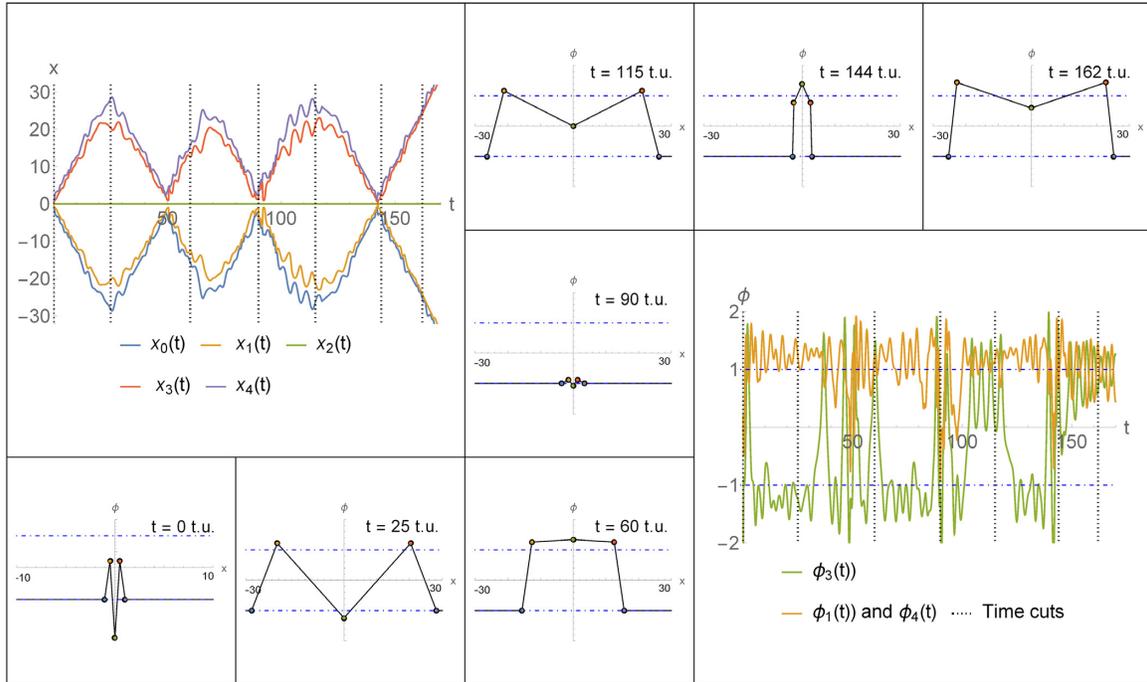
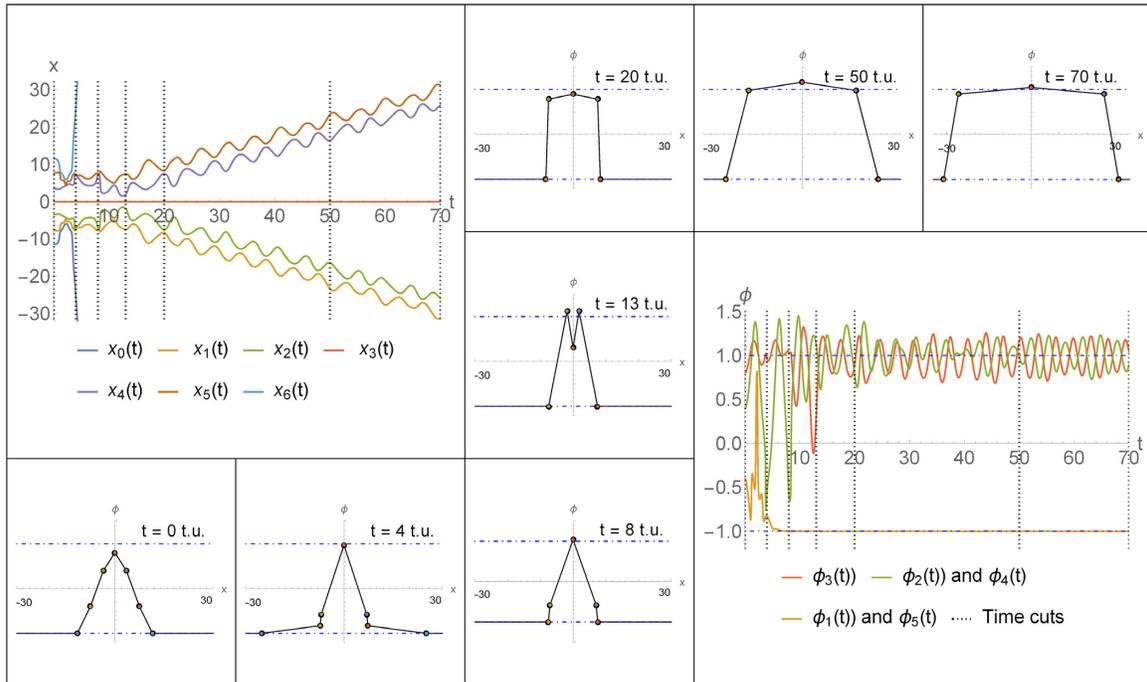**Fig. 22.** Initial "bounces" before a mech-$K\bar{K}$ ejection for an $N = 4$ mech-oscillon.

Fig. 23. An initial ejection of outermost joints followed by ejection of a highly-excited mech-$K\bar{K}$ pair for an $N = 6$ mech-oscillon.

Of course, arbitrary combinations of the above processes can occur in sequence for sufficiently high N (Figs. 17, 18, and 23).

Let us stress that mechanization should be viewed as a proof of concept rather than a serious attempt at general-purpose CCMs. Indeed, there are issues with our construction. The most

glaring one is the geodetic incompleteness of the moduli space, which is perhaps the largest source of quantitative disagreement.

As we discussed, singularities arise whenever the distance between two joints becomes zero, i.e. $\Delta x_a = 0$, or a middle segment becomes flat, i.e. $\Delta \phi_a = 0$. The second type of singularity introduces an unexpected practical problem: it is quite challenging to investigate mech-$K\bar{K}$ scattering directly. This is because the configuration of an initially separated mech-kink and anti-mech-kink with a flat segment in between is dynamically decoupled. Indeed, such a configuration is an exact solution of the equations of motion describing free particles. However, upon contact, we arrive at a $\Delta x_a = 0$ type singularity, and the equations of motion break down. For this reason, we have mostly investigated the evolution of large-N mech-oscillons that provide an indirect way of studying the scattering of mech-kinks.

The resolution of moduli space singularities would be a fundamental step forward. At present, it is not clear to us how we should accomplish this. It is telling, however, that the singularities appear whenever the mech-field suddenly changes its (effective) number of joints. For example, one may continue beyond a singular collision of a free-moving mech-$K\bar{K}$ pair, which is an $N = 3$ configuration, by replacing it with an $N = 2$ mech-oscillon. Although intuitive, it is difficult to realize this approach in practice.

In other words, we should figure out how to dynamically connect different N-sectors. Making the number of particles vary would also provide a step towards restoring explicit Lorentz covariance. There is an obvious way to achieve this that we already know, i.e. taking $N \to \infty$ and reintroducing the continuous field. Whether there exists a middle ground where N would remain a finite and discrete dynamical variable remains a tantalizing possibility.

References

1 D. K. Campbell, J. F. Schonfeld, and C. A. Wingate, Phys. D **9** 1 (1983).
2 M. Moshir, Nucl. Phys. B **185** 318 (1981).
3 T. I. Belova and A. E. Kudryavtsev, Phys D **32** 18 (1988).
4 P. Anninos, S. Oliveira, and R. A. Matzner, Phys. Rev. D **44** 1147 (1991).
5 A. Halavanau, T. Romanczukiewicz, and Y. Shnir, Phys. Rev. D **86** 085027 (2012) [arXiv:1206.4471 [hep-th]]. Search inSPIRE.
6 P. Dorey, K. Mersh, T. Romanczukiewicz, and Y. Shnir, Phys. Rev. Lett. **107**, 091602 (2011) [arXiv:1101.5951 [hep-th]]. Search inSPIRE.
7 H. Weigel, J. Phys. Conf. Ser. **482** 012045 (2014) [arXiv:1309.6607 [nlin.PS]]. Search inSPIRE.
8 M. Haberichter, R. MacKenzie, M. B. Paranjape, and Y. Ung, J. Math. Phys. **57** 042303 (2016) [arXiv:1506.05838 [hep-th]]. Search inSPIRE.

9   J. Ashcroft, M. Eto, M. Haberichter, M. Nitta, and M. B. Paranjape, J. Phys. A **49** 365203 (2016) [arXiv:1604.08413 [hep-th]]. Search inSPIRE.

10 N. S. Manton, K. Oleś, T. Romańczukiewicz, and A. Wereszczyński;, Phys. Rev. D **103** 025024 (2021) [arXiv:2008.01026 [hep-th]]. Search inSPIRE.

11 N. S. Manton, K. Oles, T. Romanczukiewicz, and A. Wereszczynski, Phys. Rev. Lett. **127** 071601 (2021) [arXiv:2106.05153 [hep-th]]. Search inSPIRE.

12 C. Adam, K. Oles, T. Romanczukiewicz, and A. Wereszczynski, Phys. Rev. D **101** 105021 (2020) [arXiv:1909.06901 [hep-th]]. Search inSPIRE.

13 C. Adam, N. S. Manton, K. Oles, T. Romanczukiewicz, and A. Wereszczynski, arXiv:2111.06790 [hep-th]. https://inspirehep.net/literature?sort=mostrecent&size=25&page=1&q=find%20eprint %202111.06790&ui-citation-summary=true&ui-exclude-self-citations=true.

14 P. G. Kevrekidis and R. H. Goodman, (2019), arXiv:1909.03128, https://inspirehep.net/literature? sort=mostrecent&size=25&page=1&q=find%20eprint%201909.03128&ui-citation-summary=tru e&ui-exclude-self-citations=true.

15 S. Wolfram, A New Kind of Science (Wolfram Media, Champaign, IL,2002).

16 N. S. Manton and P. Sutcliffe, Topological Solitons (Cambridge University Press, Cambridge, 2007).

17 E. B. Bogomolny, Sov. J. Nucl. Phys. **24** (1976).

18 N. S. Manton, Phys. Lett. B **110** 54 (1982),

19 M. J. Rice, Phys. Rev. B **28** 3587 (1983).

20 M. Gleiser, Phys. Rev. D **49** 2978 (1994), [arXiv:hep-ph/9308279]. Search inSPIRE.

21 E. J. Copeland, M. Gleiser, and H. R. Muller, Phys. Rev. D **52** 1920 (1995) [arXiv:hep-ph/9503217]. Search inSPIRE.

22 E. A. Andersen and A. Tranberg, J. High Energy Phys. **12** 016 (2012) [arXiv:1210.2227 [hep-ph]]. Search inSPIRE.

23 P. Salmi and M. Hindmarsh, Phys. Rev. D **85** (2012), 085033[arXiv:1201.1934 [hep-th]]. Search in SPIRE.

24 P. M. Saffin and A. Tranberg, J. High Energy Phys. **01** (2007), 030[arXiv:hep-th/0610191]. Search in SPIRE.

25 G. Fodor, P. Forgacs, P. Grandclement, and I. Racz, Phys. Rev. D **74** (2006), 124003[arXiv:hep-th/0609023]. Search inSPIRE.

26 M. Gleiser and D. Sicilia, Phys. Rev. D **80** 125037 (2009) [arXiv:0910.5922 [hep-th]]. Search inSPIRE.

27 J. Olle, O. Pujolas, and F. Rompineve, J. Cosmol. Astropart. Phys. **09** 015 (2021) [arXiv:2012.13409 [hep-ph]]. Search inSPIRE.

28 C. Adam, K. Oles, T. Romanczukiewicz, and A. Wereszczynski, Phys. Rev. Lett. **122** 241601 (2019) [arXiv:1903.12100 [hep-th]]. Search inSPIRE.